

NASA/TM-2018-219835



Mitigation of Polystyrene Microsphere Surface Contamination for Wind Tunnel Applications

*Christopher J. Wohl, Pacita I. Tiemsin, Samuel J. Robbins, and Ashle Page
Langley Research Center, Hampton, Virginia*

June 2018

NASA STI Program . . . in Profile

Since its founding, NASA has been dedicated to the advancement of aeronautics and space science. The NASA scientific and technical information (STI) program plays a key part in helping NASA maintain this important role.

The NASA STI program operates under the auspices of the Agency Chief Information Officer. It collects, organizes, provides for archiving, and disseminates NASA's STI. The NASA STI program provides access to the NTRS Registered and its public interface, the NASA Technical Reports Server, thus providing one of the largest collections of aeronautical and space science STI in the world. Results are published in both non-NASA channels and by NASA in the NASA STI Report Series, which includes the following report types:

- **TECHNICAL PUBLICATION.** Reports of completed research or a major significant phase of research that present the results of NASA Programs and include extensive data or theoretical analysis. Includes compilations of significant scientific and technical data and information deemed to be of continuing reference value. NASA counter-part of peer-reviewed formal professional papers but has less stringent limitations on manuscript length and extent of graphic presentations.
- **TECHNICAL MEMORANDUM.** Scientific and technical findings that are preliminary or of specialized interest, e.g., quick release reports, working papers, and bibliographies that contain minimal annotation. Does not contain extensive analysis.
- **CONTRACTOR REPORT.** Scientific and technical findings by NASA-sponsored contractors and grantees.

- **CONFERENCE PUBLICATION.** Collected papers from scientific and technical conferences, symposia, seminars, or other meetings sponsored or co-sponsored by NASA.
- **SPECIAL PUBLICATION.** Scientific, technical, or historical information from NASA programs, projects, and missions, often concerned with subjects having substantial public interest.
- **TECHNICAL TRANSLATION.** English-language translations of foreign scientific and technical material pertinent to NASA's mission.

Specialized services also include organizing and publishing research results, distributing specialized research announcements and feeds, providing information desk and personal search support, and enabling data exchange services.

For more information about the NASA STI program, see the following:

- Access the NASA STI program home page at <http://www.sti.nasa.gov>
- E-mail your question to help@sti.nasa.gov
- Phone the NASA STI Information Desk at 757-864-9658
- Write to:
NASA STI Information Desk
Mail Stop 148
NASA Langley Research Center
Hampton, VA 23681-2199

NASA/TM-2018-219835



Mitigation of Polystyrene Microsphere Surface Contamination for Wind Tunnel Applications

*Christopher J. Wohl, Racita I. Tiemsin, Samuel J. Robbins, and Ashle Page
Langley Research Center, Hampton, Virginia*

National Aeronautics and
Space Administration

Langley Research Center
Hampton, Virginia 23681-2199

June 2018

Acknowledgments

The author would like to thank the support of: Frank Palmieri, Scott Bartram, Harold Claytor, Wes Tayon, Michael Oliver, James Baughman, Eric Hoffman, and Paul Bagby from NASA Langley Research Center; Jan Genzer and Russell Schmitz from North Carolina State University; Zoe Arthur, Bryce Connelly, Sarah Hopkins, Alexandra Bosh, and the NASA Internship, Fellowship, and Scholarship (NIFS) Program coordinators.

The use of trademarks or names of manufacturers in the report is for accurate reporting and does not constitute an official endorsement, either expressed or implied, of such products or manufacturers by the National Aeronautics and Space Administration.

Available from:

NASA STI Program / Mail Stop 148
NASA Langley Research Center
Hampton, VA 23681-2199
Fax: 757-864-6500

Abstract

Polystyrene latex (PSL) microspheres have been utilized as seed material for flow visualization in wind tunnels. However, PSL microspheres have been observed to strongly adhere to wind tunnel and model surfaces. Surface contamination on the cleaning screens that remove vorticity and provide laminar flow in the test section, is particularly problematic. Agglomeration of particles on these screens cause constriction of the airflow through the screen resulting in inconsistent airflow properties in the test section. The adhesion mechanism of PSL microspheres to wind tunnel screens and 316 stainless steel flat plates, were evaluated in a contamination apparatus where small sections of screen material were exposed to PSL-seeded airflow. Using a design of experiments (DOE) methodology airflow seeding parameters were changed to evaluate how these modifications affected the degree of surface contamination. The solution composition, comprised of ethanol and water, was determined to be the most significant factor in particle adhesion. Utilizing image analysis software, data were collected from the contaminated surfaces and incorporated to generate predictive particle contamination models. A relationship was identified between the solvent evaporation rate, and the morphology and magnitude of PSL contaminants on the test surfaces. This analysis can be extended to other solvent mixtures to provide insight into simultaneously improving wind tunnel testing capabilities while diminishing facility contamination.

Table of Contents

Abstract	1
Table of Contents	2
Table of Tables	3
Table of Figures	4
Introduction.....	5
Experimental	7
Materials and Equipment	7
PSL Solution Generation	7
Contamination Rig	7
Screen Contamination Experiments.....	8
Design of Experiments Study of Aluminum Surface PSL Contamination	11
Environmental Condition Determination for Liquid Droplet Evaporation Calculations	12
Results and Discussion	12
Contamination of Stainless Steel Screens.....	12
Contamination of Polished Aluminum Surfaces.....	14
Dependence of Solvent Composition on Surface Contamination.....	15
Dependence of Nozzle and Vessel Pressure Ratio on Surface Contamination.....	21
Contamination Experiments with Fluorescent Dye Containing Solutions.....	23
Verification Experiments on Stainless Steel Screen Samples.....	23
Thermodynamic Analysis of Liquid Droplet Evaporation.....	24
Conclusion and Outlook	26
References.....	26
Appendix A: Image Analysis and Verification.....	28
Image Analysis Methodology	28
Image Analysis Validation.....	30
Appendix B: Design of Experiments Data and Statistical Analysis	31
Appendix C: Mathematica Code for Determination of Droplet Evaporation Rate.....	34
Appendix D: Measured Airspeed and Relative Humidity Values in the Contamination Rig.....	45

Table of Tables

Table 1. Screen contamination test conditions.....	9
Table 2. Aluminum alloy flat plate coupon roughness and resultant PSL areal coverage.....	11
Table 3. DOE inputs and values.....	11
Table 4. Calculated distance required for complete solvent evaporation.	25

Table of Figures

Figure 1. (A) Example of PIV wind tunnel experimental set-up. (B) Example of a resultant flow vector field generated via PIV experimentation conducted at NASA Langley Research Center.	5
Figure 2. (A) Cleaning screen location in a closed return wind tunnel. (B) Cleaning screens enable laminar flow with consistent flow properties to enter the test section. ⁹	6
Figure 3. (A) Image of cleaning screens located in the 14 by 22 FT ST. (B) Closer image of the cleaning screens indicating the morphology of the screen (wire) surfaces.	6
Figure 4. Particle size distribution of the stock PSL solution utilized in this work.	7
Figure 5. Labeled image of the contamination rig utilized to evaluate PSL surface contamination.....	8
Figure 6. Labeled image of the pressure vessel that contained the PSL seed solution.	8
Figure 7. Configuration for screen coupon contamination testing.....	9
Figure 8. Position of screen coupons for contamination testing.	9
Figure 9. Examples of contaminated screen images captured using (A) a high resolution camera, (B) an optical microscope, and (C) an optical microscope equipped with a motorized z-stage for extended focus image processing and mosaic image stitching.	10
Figure 10. Screen morphology numbering scheme.....	10
Figure 11. Sample orientation for DOE contamination study.....	11
Figure 12. Images of screens located at position 1 contaminated with PSLs at increasing exposure duration.	13
Figure 13. PSL contamination at Micro position 2 for screens located in position 1 that were exposed to (A) 1 s, (B) 5 s, (C) 30 s, (D) 60 s, and (E) 5 minutes, respectively.	13
Figure 14. PSL contamination at Micro position 10 for screens located in position 3 that were exposed to (A) 1 s, (B) 5 s, (C) 30 s, (D) 60 s, and (E) 5 minutes, respectively.	13
Figure 15. PSL contaminant structures arising from surface interaction.....	14
Figure 16. Representative images for PSL deposits observed on (A) as-received Al 6061 and (B) polished Al 6061 coupon surfaces.....	15
Figure 17. (A) PSL contaminant % areal coverage vs roughness. (B) Schematic illustrating increased potential for PSL surface interactions near surface roughness elements.	15
Figure 18. Major PSL contaminant structures observed on polished Al 6061 flat plates. Images were captured at 5x magnification.....	17
Figure 19. Correlation between contamination data series 1 (filled circles) and 2 (open circles). The fit lines are continuous and dashed for data series 1 and 2, respectively.	18
Figure 20. Solvent composition and run time image compilation for contamination experiments conducted at an N:T of 6.	19
Figure 21. Solvent composition and run time image compilation for contamination experiments conducted at an N:T of 12.	19
Figure 22. Actual and predicted model results for correlation of % areal coverage.....	20
Figure 23. 3D surface of modeled surface contamination as a function of run time and solvent composition.....	21
Figure 24. Optical micrographs collected at solvent ratios (EtOH:H ₂ O) ratios of: (A) 0:1, (B) 1:1, and (C) 1:0). Run times and N:T are indicated in each series of images.	22
Figure 25. 3D surface of modeled surface contamination as a function of N:T and solvent composition.	22
Figure 26. Rinse water under UV illumination from contamination experiment surfaces exposed to spray by solvents containing Kiton red. EtOH:H ₂ O ratios were: (left) 0:1, (middle) 1:1, (right) 1:0.	23
Figure 27. (A) Uncontaminated stainless steel screen. (B) A stainless steel screen exposed to 1:0 (EtOH:H ₂ O) PSL solution spray. (C) A stainless steel screen exposed to 0:1 (EtOH:H ₂ O) PSL solution spray.....	24
Figure 28. The time dependence for a 4 μm droplet of different solvent composition to evaporate.	25

Introduction

Polystyrene microspheres (PSL)s have been demonstrated to be an ideal seed material for flow visualization techniques (e.g., particle image velocimetry (PIV), and laser Doppler velocimetry, etc.) in liquid and gaseous flows.¹⁻² This is a result of their relatively low density, small aerodynamic diameter (rapid response time to airflow velocity change), and high refractive index. Additionally, PSLs are relatively soft compared to alumina or other solid seed materials, and can be readily acquired as a monodisperse material compared to other droplet seed materials that may have broad size distributions.³ Knowledge of the PSL diameter *a priori* is also advantageous and unique compared to other droplet seed materials. Combined, these properties produce a readily detectable scattered laser light with little uncertainty between the calculated and actual airflow properties.⁴⁻⁵ Beyond light scattering for signal transduction, multifunctional PSLs have been utilized to provide further insight into flow properties deeper into the boundary layer than possible with traditional PIV techniques.⁶⁻⁸

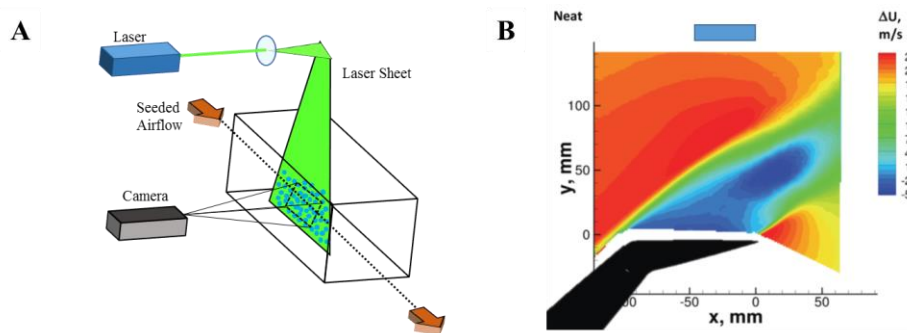


Figure 1. (A) Example of PIV wind tunnel experimental set-up. (B) Example of a resultant flow vector field generated via PIV experimentation conducted at NASA Langley Research Center.

Unfortunately, PSL microspheres exhibit strong adhesion to wind tunnel surfaces. Adhesion of the microspheres is especially pernicious toward wind tunnel cleaning screens (flow conditioning screens). The position of flow conditioning screens just before the test section is shown in a schematic of a closed return wind tunnel in Figure 2A. Air exiting the fans often exhibits significant turbulence; these screens are designed to “clean” the air by providing laminar flow in the test section. As air passes through the openings of the screens, turbulent flow is reduced to uniform laminar flow prior to entering the test section. A schematic of the “cleaning” process of airflow via flow conditioning screens is shown in Figure 2B.

The flow conditioning screens of particular interest in this work are utilized at the NASA Langley Research Center 14 ft by 22 ft sub-sonic wind tunnel facility (14 by 22 FT ST) (Figure 3A). They are composed of 0.0225 in diameter stainless steel wires woven into an arrangement of 0.125 in x 0.125 in openings (Figure 3B). Although PSLs exhibit preferential characteristics regarding flow visualization, strong intrinsic adhesion to wind tunnel surfaces, especially these cleaning screens, often detract from their utility and may prevent the use of PSLs. These screens are located between the seeding mechanism and the test section in the current configuration of the NASA Langley 14 by 22 FT ST facility, and exhibit particle contamination after conducting PIV experiments in which PSLs are utilized. Consequences of this contamination can result in significant down time of the facility and can exceed more than \$100,000 in cleaning costs. Beyond monetary and aesthetic considerations, particle contamination can alter the uniformity of the screen openings affecting airflow properties in the test section. Identifying readily accessible methods to introduce the PSLs that reduce the extent of surface contamination would be of great utility.

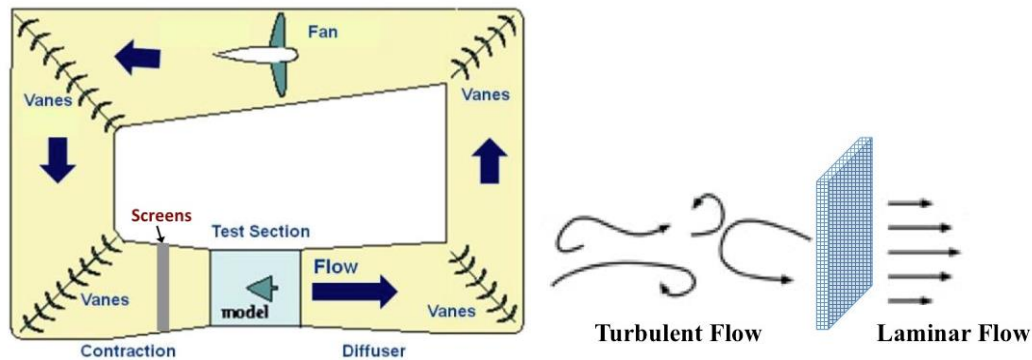


Figure 2. (A) Cleaning screen location in a closed return wind tunnel. (B) Cleaning screens enable laminar flow with consistent flow properties to enter the test section.⁹

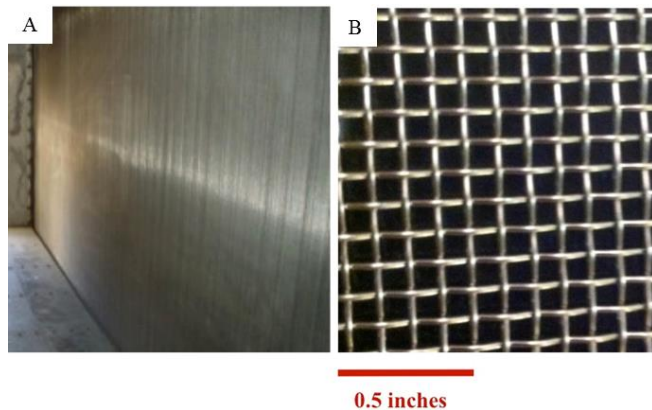


Figure 3. (A) Image of cleaning screens located in the 14 by 22 FT ST. (B) Closer image of the cleaning screens indicating the morphology of the screen (wire) surfaces.

In this work, the mechanisms of PSL adhesion to surfaces was evaluated using a custom-built contamination rig. This was achieved by seeding air drawn through the contamination rig from an ultrasonic nozzle identical to the ones utilized in the 14 by 22 FT ST facility. Initial experiments were conducted utilizing standard PSL solution compositions and seed delivery methods in order to recreate contamination scenarios on screen surfaces identical to those present in the actual facilities. Once these contaminated surfaces were characterized and the mechanism of PSL adhesion was determined, the surface to be contaminated was changed to determine the substrate composition influence. Likewise, a design of experiments (DOE) was utilized to address the contribution from various experimental parameters including: seeded air pressure, liquid/air pressure ratio, spray duration, and solvent composition. These results were compiled and statistical analysis was performed to determine the most significant contribution to surface contamination: solvent composition, which was related to a change in evaporation rate. To bridge the gap from theoretical to experimental, a brief investigation into the thermodynamic behavior of small liquid droplets and their evaporation rates was conducted. This analysis can be applied to other solvent compositions not currently being utilized for PSL delivery methods.

Experimental

Materials and Equipment

The PSLs utilized here were generated at NASA Langley Research Center using surfactant free emulsion polymerization.³ The particle size distribution shown in Figure 4 was determined using a dynamic light scattering instrument (Particle Sizing Systems Accusizer 780 AD). The particle mean diameter was $1.27 \pm 0.43 \mu\text{m}$. Although the standard deviation appears large, particles associated with the peak around $0.5 \mu\text{m}$ will not be relevant for PIV measurements as they are below the detection threshold for most experimental configurations.

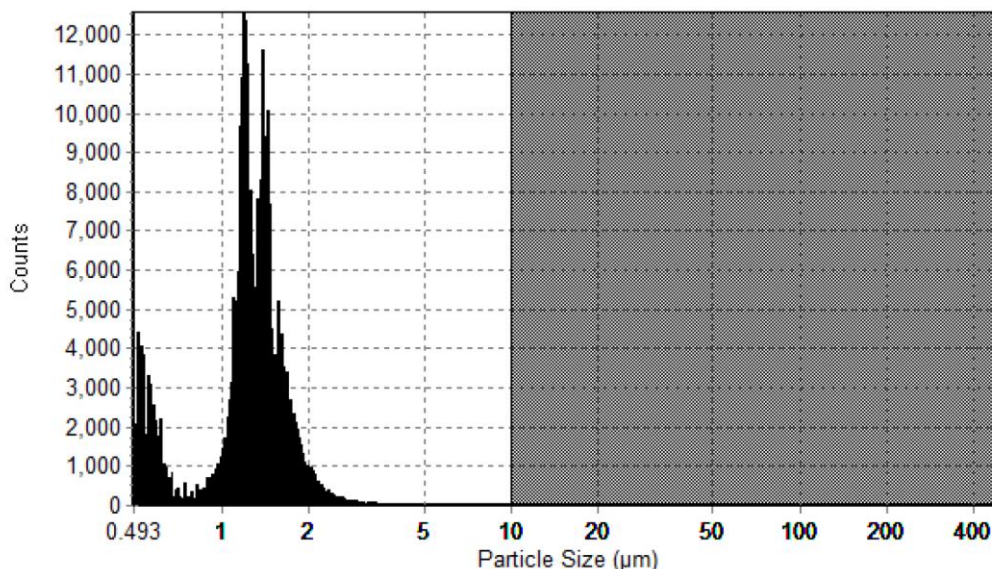


Figure 4. Particle size distribution of the stock PSL solution utilized in this work.

High-resolution images were captured immediately after contamination experiments using a Nikon D800E. Optical microscopy images were captured using a Leica DM8000M with additional contaminant-substrate contrast achieved using a Fiber-Lite optical illuminator. Height-resolved optical microscopy images were captured using Zeiss LSM 5 Exciter microscope with AxioVision 4.8 software which contained extended focus algorithms and image stitching functions.

PSL Solution Generation

PSL seed solutions were generated by dilution of the aqueous PSL stock solution (9 wt% solids) into different ethanol:water solvent mixtures (ranging from pure water to pure, 200 proof, ethanol) at a ratio of 1:10 PSL solution:solvent. Typical EtOH:H₂O solvent mixtures utilized in wind tunnel testing are 1:1.

Contamination Rig

PSL surface contamination tests were conducted using a custom-built particle contamination assembly designed to emulate conditions found in 14 by 22 FT ST. The particle contamination assembly was approximately 41.5 in length, 22.5 in width, and 22 in height (Figure 5) and consisted of a small opening in front, a Plexiglas door on one side, and a ventilation channel through the back. An ultrasonic nozzle (Sonicom model 035H-N) was placed at the front opening. Three channels that held 18 in by 18 in 316 stainless steel screens (10 mesh, 0.025 in wire diameter) identical to the ones utilized in 14 by 22 FT ST were spaced approximately 25 in, 32 in, and 40 in from the ultrasonic nozzle. An EBAC PF400 fan with an airflow (free air) of $3700 \text{ m}^3 \text{ hr}^{-1}$ was used to draw air into the tunnel.



Figure 5. Labeled image of the contamination rig utilized to evaluate PSL surface contamination.

PSL mixtures were poured into a pressure-controlled stainless steel vessel (Figure 6). The PSL solution-containing vessel was connected to the Sonicom ultrasonic nozzle. Connected to both the vessel and the nozzle via manifold was a central line of compressed air (70-85 psi). Testing was performed outside to allow for maximum ventilation of the polystyrene microparticles.

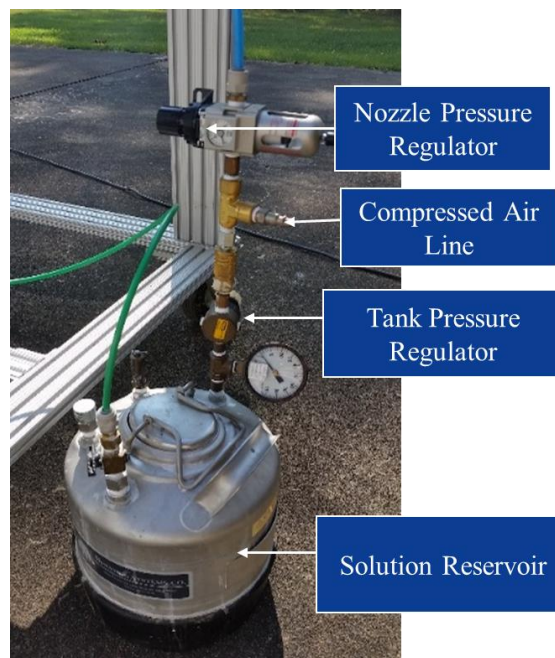


Figure 6. Labeled image of the pressure vessel that contained the PSL seed solution.

Screen Contamination Experiments

Stainless steel screen coupons (4 in x 4 in coupons) were attached to the larger screens in the contamination rig (Figure 7) at the first and third screen position (Figure 8) and exposed to the PSL seed solution for a discrete amount of time ranging from 1-300 seconds (Table 1). The wall pressure for all of these experiments was 70 psi and the nozzle/tank pressure ratio was 8:1. For these experiments, samples were exposed individually, i.e., testing occurred at each screen location with no other screen samples present. This was done in order to prevent any type of shielding or masking from occurring as a result of test articles placed upstream from a sample location.

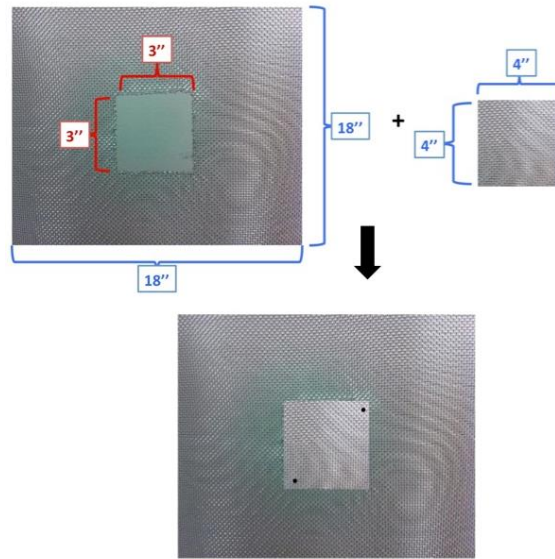


Figure 7. Configuration for screen coupon contamination testing.



Figure 8. Position of screen coupons for contamination testing.

Table 1. Screen contamination test conditions.

Sample	Screen Position	Exposure Duration (s)
1-A	1	1
1-B	1	5
1-C	1	30
1-D	1	60
1-E	1	300
2-A	3	1
2-B	3	5
2-C	3	30
2-D	3	60
2-E	3	300

Following testing, particle contamination was characterized using high-resolution photography and optical microscopy (Figure 9). Traditional optical microscopy was only effective within limited regions as the curvature of the screens contributed to blurry images.

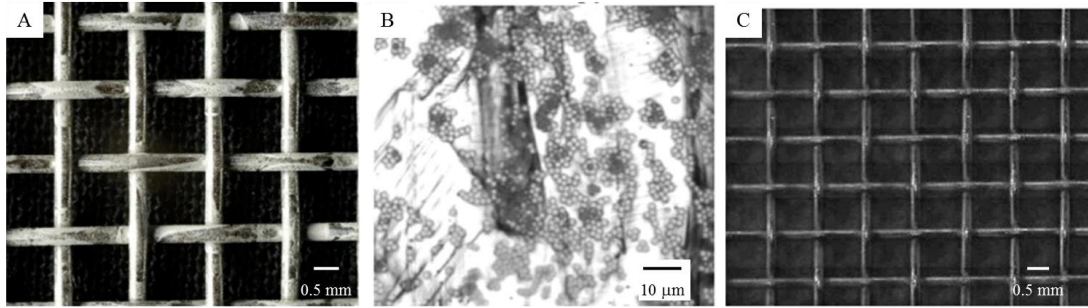


Figure 9. Examples of contaminated screen images captured using (A) a high resolution camera, (B) an optical microscope, and (C) an optical microscope equipped with a motorized z-stage for extended focus image processing and mosaic image stitching.

Due to the complexity of the screen surface, a numbering system was generated to account for the screen morphology (Figure 10). Three general regions were identified: intersections where the vertical wire overlaid the horizontal wire, intersections where the horizontal wire overlaid the vertical wire, and wire located away from intersections (herein referred to as intermediate wire). This enabled identification of any morphology-dependent aerosolized PSL suspension/screen interactions.

Micro-Regional Nomenclature

- Vertical Overlay (#1-5)
- Horizontal Overlay (#6-10)
- Intermediate Wire (#11)

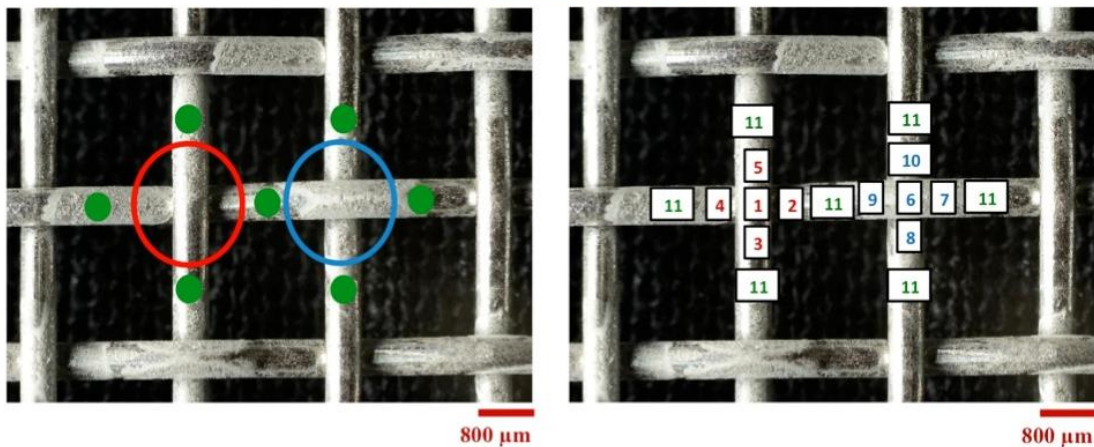


Figure 10. Screen morphology numbering scheme.

Additional experiments were conducted on aluminum alloy (Al 6061) flat plate coupons (2 in × 2 in) to evaluate the influence surface roughness has on particle retention (Table 2). An Al 6061 coupon was tested as received. Another sample was polished using a Buehler parallel plate motorized polisher using 320, 400, 600, 800, and 1200 grit silicon carbide (SiC) paper. The sample was polished at each grit level for 90 seconds, four times, alternating clockwise and counterclockwise directions for each grit at sequentially increasing grit number. In between each grit step, the samples were gently rinsed with water to remove any residue. For testing in the contamination rig, the wall pressure and nozzle:tank ratio (N:T) were 70 psi and 8:1. The samples were affixed to the screen in position 1 and were exposed for 30 seconds.

Table 2. Aluminum alloy flat plate coupon roughness and resultant PSL areal coverage.

Sample	Roughness, R_a (μm)	Areal Coverage (%)
As-received Al 6061	0.54±0.03	59±11
Polished Al 6061	0.02±0.005	12±8

Design of Experiments Study of Aluminum Surface PSL Contamination

A design of experiments approach (utilizing Design Expert 9, Stat-Ease), was used to determine how various aspects of PSL seed airflow delivery influence surface contamination. Using this approach, the variable space (the possible combinations of inputs) was studied in such a manner that the results (returns) can be evaluated against each input individually, or in combination, across the full range of input conditions. Table 3 shows the variables that were investigated in this study. Six experimental parameters were examined. Seed solution composition was varied to ascertain solvent evaporation during PSL travel. The overall air pressure was varied to change the total air mass (including seed-laden volume) delivered to the contamination rig. Variation of the nozzle/tank pressure enabled determination of the influence that the portion of the air mass containing seed material had on surface contamination. Changing the seed delivery duration was performed to evaluate cumulative effects on surface contamination. Test coupons were held in place by a paperclip on the 18 in by 18 in screens inside the tunnel at position 1 or position 3 to change the PSL travel distance prior to sample interaction (Figure 8). Different coupon locations were utilized to enable determination of the influence of test variables on PSL seed cloud uniformity (Figure 11). Only a single return parameter (mean particle coverage, %) was utilized in these experiments. See Appendix B for a table of input conditions and return values for all experiments defined by the DOE.

Table 3. DOE inputs and values.

Input	Values				
Seed solution composition (EtOH:H ₂ O ratio)	0:1	1:3	1:1	3:1	1:0
Air pressure (psi)	70	85			
N:T*	6:1	8:1	12:1		
Seed delivery duration** (s)	10-60				
Screen position	1	3			
Coupon location	1	2	3		

*Values correspond to the ratio of nozzle pressure to tank pressure with reference to the corresponding compressed air pressure values

**For this DOE configuration, all inputs were set to discrete values except seed delivery duration.

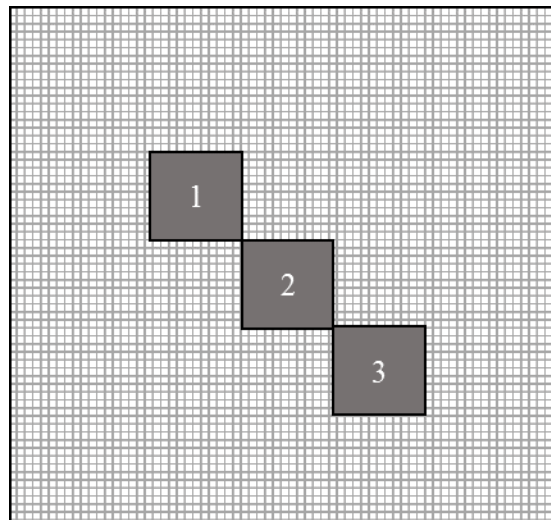


Figure 11. Sample orientation for DOE contamination study.

Contamination experiments were conducted on aluminum alloy (Al 6061) coupons (3 in by 3 in). This substrate was selected as it would enable more quantitative analysis of the contamination level, relative to the screen surfaces which had both a complex morphology and significant open spaces. Prior to testing, each sample was mechanically polished to minimize surface defects that may influence PSL deposition processes as described above.¹⁰⁻¹²

Testing was conducted over a span of 30 days and was performed outside for maximum ventilation of the PSL solution. Temperature and humidity variations were not taken into account during these tests, and as a result, data may be impacted by these uncontrollable variables. For each PSL solution composition, a total of 400 mL of solution was generated to ensure enough material was available to complete all of the experiments without generation of multiple solutions of the same target composition. A second set of experimental conditions were evaluated (Data Series 2) to provide further insight into the influence that N:T has on surface contamination. To limit other contributing factors in Data Series 2, samples were tested at screen position 1, substrate orientation 2, and at a central pressure of 85 PSI. Tests were conducted at 10, 30, or 60 second run times and at 6:1 or 12:1 N:T pressure ratios. Following all testing, the substrates were characterized using optical microscopy and ImageJ software (Image Processing and Analysis in Java, see Appendix A for description of analytical method).

To further investigate solvent solution drying properties, tests were conducted without incorporation of PSLs. A fluorescent dye solution was generated from 50 mg of kiton red 620 dye and 5 mL of ethanol. From this solution, 200 μ L was added to 300 mL of a 0:1, 1:1, and a 1:0 200 proof ethanol/water mixture. Each solution was seeded into the contamination rig for 30 seconds at 70 psi, screen position 1, and substrate orientation 2. Each solution was tested once at 6:1 and 12:1 N:T. Any seeded solution droplets that had not completely evaporated prior to interacting with the Al alloy coupon would result in dye deposition. It was assumed that nominal dye deposition would occur with complete solvent evaporation prior to coupon impact. The samples were placed in a drying chamber overnight. In order to examine the residual water soluble dye present on the coupon surfaces, 5 mL of water was carefully placed onto the samples via pipet and maneuvered to wet the entire surface. This rinse water was collected in test tubes to observe the fluorescent emission from the solvated dye. A hand-held UV light illuminated the test tubes ($\lambda=365$ nm) and high-resolution images were captured with a Nikon D800E digital camera.

Environmental Condition Determination for Liquid Droplet Evaporation Calculations

Calculation of evaporation rates required knowledge of air speed and solution flow rate. An air speed of 2,500 ft min⁻¹ was measured at the nozzle exit using an anemometer (Q-Trak Model 7575). The flow rate of the Sonicom nozzle at 6:1 and 12:1 nozzle/tank pressure ratios was determined by measuring the time required to disperse 300 mL of water from the nozzle. A PSL solution flow rate of 4.2 L hr⁻¹ and 3.3 L hr⁻¹ was measured at pressure ratios of 6:1 and 12:1.

Results and Discussion

Contamination of Stainless Steel Screens

Based on studies conducted in 14 by 22 FT ST at NASA Langley Research Center, PIV measurements utilizing PSLs as seed material result in extensive contamination of the cleaning screens. To fundamentally understand how this contamination was initiated, designed screen contamination experiments were conducted in a contamination rig that reproduces the conditions experienced in 14 by 22 FT ST.

A series of screen samples were tested in the first position, closest to the particle release nozzle. Approximately 22 in from the release point of the particles, the screens were highly contaminated after one second (Figure 12). PSL solution was readily visible on the screen surfaces after each contamination trial when the duration time was 30 seconds or greater. The solution appeared to concentrate at the wire overlay points. PSL solution dripped off the screen samples at exposure durations of 60 seconds or

greater. An additional series of samples were exposed in the third position, the position furthest from the nozzle (approximately 40 in). At this position, screens exhibited less contamination during the same exposure duration as those tested in the first position, described in greater detail below using microscopy images. Dripping of PSL solution, however, remained present especially after 300 s exposure.

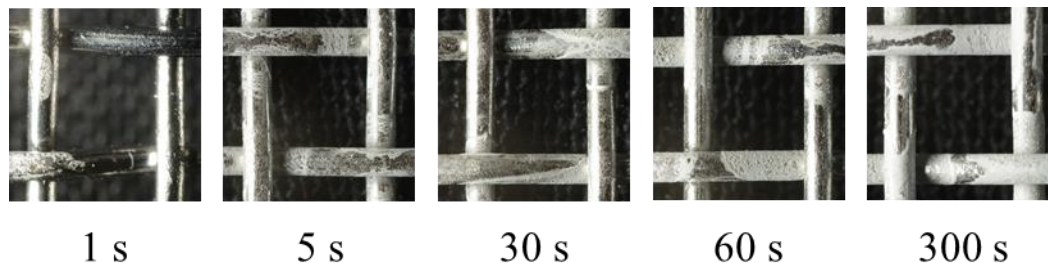


Figure 12. Images of screens located at position 1 contaminated with PSLs at increasing exposure duration.

The samples tested in this study exhibited similar trends in particle adhesion. No noticeable mechanical deformation of PSL microspheres was present as particles retained their spherical form following testing. Adhesion between microparticles was likely due to intermolecular van der Waals forces. In general, screens contaminated according to the conditions in Table 1 exhibited less particle contamination at the apex of wires, (Micro 1 and 6 positions in Figure 10) in comparison to the curved sides of the wires. Regions near intersections (Micro #2-5, 7-10) contained larger particle multilayers (Figure 13). At intermediate positions along screen wires (Micro #11), adhesion results were highly variable, exhibiting few particles to almost 100% multilayer coverage. Contamination levels were observed to be lower for samples placed in the 3rd screen position (Figure 14), relative to those in the 1st screen position. As can be seen in Figures 14C and D, at intermediate exposure times circular deposits were observed on samples contaminated in the 3rd screen position. These “coffee-ring effect” deposits, as well as other general forms of contamination will be discussed next. These features were not as prevalent for samples contaminated in the 1st position.

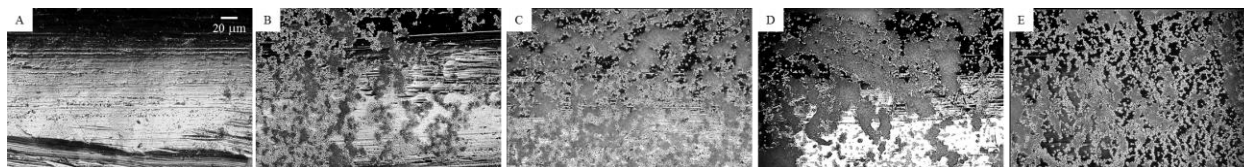


Figure 13. PSL contamination at Micro position 2 for screens located in position 1 that were exposed to (A) 1 s, (B) 5 s, (C) 30 s, (D) 60 s, and (E) 5 minutes, respectively.

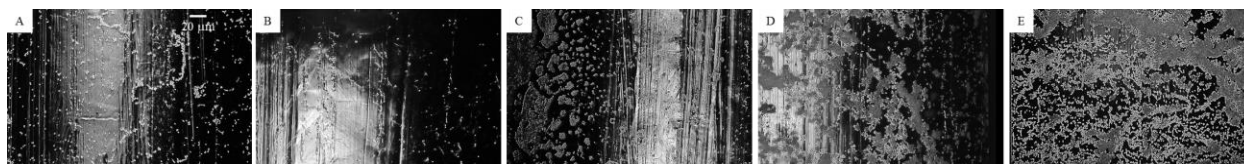


Figure 14. PSL contamination at Micro position 10 for screens located in position 3 that were exposed to (A) 1 s, (B) 5 s, (C) 30 s, (D) 60 s, and (E) 5 minutes, respectively.

PSL deposits were observed to consist of several different multi-particle configurations. Random deposition resulted in generation of scattered particles and multi-layered deposits, as has been indicated in previous images. Other particle configurations were observed that were indicative of specific interactions with the contaminated metal surface. In several instances, PSLs were observed preferentially oriented within surface defects (Figure 15A). The 316L grade stainless steel used for wind tunnel screens has a

surface energy of approximately 40 mJ m^{-2} which contributes to PSL adhesion.¹³ Microstructural features of the stainless steel including grain boundaries and defects resulting from fabrication provide sites of even greater surface energy, and may have contributed to the specific agglomeration of PSLs within these regions.

Another frequently observed multi-particle configuration was a band, or multiple concentric bands, of high PSL density regions (Figure 15B). The similarity of these deposits to those observed as a result of Marangoni flow¹⁴⁻¹⁶ of particles suspended in solution indicated that seeding airflows from PSL solutions comprised of a 1:1 EtOH:H₂O ratio did not result in “dry” PSLs prior to interaction with the screen surfaces. Marangoni flow within a liquid droplet arises from the greater velocity of liquid toward the contact line between the droplet and the surface. This convective flow carries any suspended material with it that concentrates at the droplet perimeter. Once the droplet has evaporated, contact line pinning keeps the droplet diameter constant until the energetic costs to maintain that diameter exceed those to “dewet” the surface, resulting in droplet retraction. The droplet will retract to a new equilibrium position that will be offset from the previous position, which is why particle deposition as a result of Marangoni flow can appear as a series of concentric bands referred to as “coffee rings.” Observation of these types of multi-particle configurations on the screen surfaces indicated that fluid droplets were deposited. This could significantly increase the PSL adhesion strength to the metal surface, due to particle mobility within the liquid droplet, enabling a more stable surface orientation. Beyond surface contamination, observation of these deposits indicates that the seeded particle diameter, utilized for fluid flow calculations, may actually be larger than the PSL diameter. Therefore, addressing the issue of solvent evaporation could enable more accurate tracking of airflow properties through a wind tunnel test section.

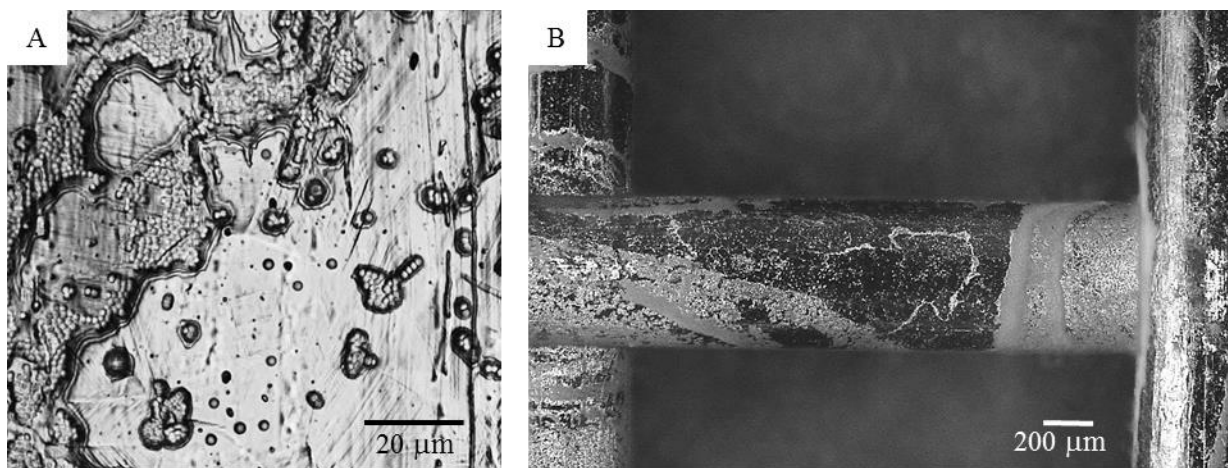


Figure 15. PSL contaminant structures arising from surface interaction

Contamination of Polished Aluminum Surfaces

From the analysis of the contaminated screen surfaces, two primary factors appeared to contribute to PSL adhesion: surface defects and deposition of solution droplets. To further elucidate the contributions from each of these factors, flat aluminum sample plates were contaminated with PSLs in the contamination rig at screen position 1. One of the samples was utilized “as-received” and another was polished, roughness values for both of these samples are indicated in Table 2. By comparing the nature and magnitude of PSL contamination on each sample, the influence of surface roughness was evaluated. Micrographs taken of both surfaces indicated a significantly greater amount of individual or small clusters of PSLs on the as-received surface, while PSLs present on polished surface were predominantly localized in the circular “coffee-ring” architectures (Figure 16).

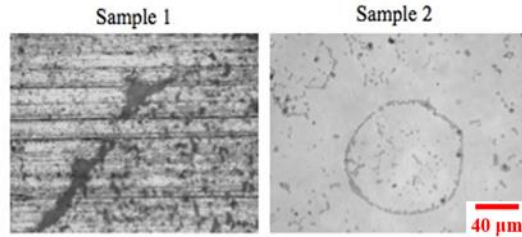


Figure 16. Representative images for PSL deposits observed on (A) as-received Al 6061 and (B) polished Al 6061 coupon surfaces.

The reduction in PSL contamination levels was quantitatively determined from these images using ImageJ area fraction analysis (Figure 17A). This analysis, described in Appendix A, indicated that the as-received Al 6061 plate retained a significantly greater amount of particle contamination with % area ranging from approximately 40-75%. Analysis of the polished Al 6061 plate yielded area fraction values from approximately 4-25%. The greater retention of PSLs on the roughened surface can be understood by considering potential contact points between the single micrometer-sized PSLs, and the as-received Al 6061 plate surface roughness (Figure 17B). Surface features, particularly from fabrication and machining, enabled two points of contact between the contaminating PSL and the surface.¹⁷ This increased adhesion and eventual agglomeration of the PSL particles. Removal of these features, as a result of polishing, reduced particle coverage due to the reduced interaction area between the PSL and Al 6061 surface. The prevalence of coffee-ring deposits on the polished surface, indicated that solvent volatility played a significant role in PSL contamination. Likewise, as removal of surface defects from the screen materials, utilized in large-scale wind tunnels, was not a feasible solution. Addressing enhanced PSL surface contamination as a result of incomplete solvent evaporation was considered to be a more practical area for improvement.

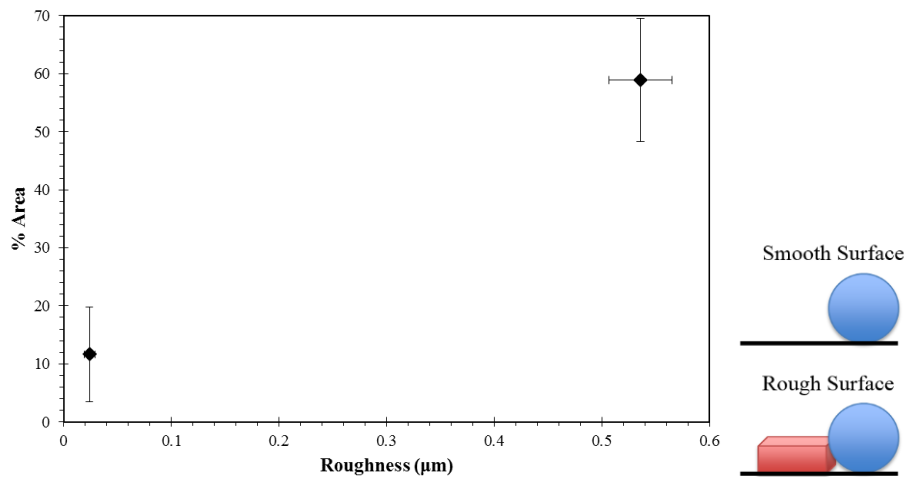


Figure 17. (A) PSL contaminant % areal coverage vs roughness. (B) Schematic illustrating increased potential for PSL surface interactions near surface roughness elements.

Dependence of Solvent Composition on Surface Contamination

Based on the contamination studies previously described, solvent-free PSL particles were not present in the airstream at the location of the cleaning screens. Instead, aerosolized solution containing PSLs was contacting the contaminated surface. Several experimental parameters contributed to the nature of the material in the airstream. The parameters evaluated in this work included solvent composition, total pressure utilized to seed the airflow, N:T, and the distance from the seed source (the ultrasonic nozzle)

and the contamination site. DOE-guided experimentation was utilized to navigate this design space. This approach enables several variables to be changed simultaneously such that, at the completion of the requisite testing, the influence that each variable independently and collectively has on specified return parameters (results) can be ascertained. Although several different methods were investigated to quantitatively evaluate the change in substrate properties, i.e., contamination level, as a result of PSL contamination; ultimately optical microscopy was the only technique determined to provide reliable results. Appendix B contains a full list of testing trials and their corresponding average particle coverage values.

Based on analysis of the body of data generated from these experiments, several general observations were made. Immediately after completion of a contamination experiment, samples generated from PSL seed solution that was 0:1 and 1:3 EtOH:H₂O appeared to have the greatest amount of liquid present as indicated by the presence of numerous large droplets. Longer run times combined with higher water concentration resulted in denser coverage that resulted in PSL solution dripping off the substrates. In contrast, samples generated from 1:1, 3:1, and 1:0 EtOH:H₂O solutions appeared uniformly dry immediately after contamination testing.

In general, samples tested at screen position 1 and for longer run times showed greater particle coverage than samples at screen position 3. Due to the concentric shape of the ultrasonic nozzle's spray pattern, samples located in orientation 2 received the most uniform PSL coverage. In a few cases, samples located at position 1 and 3 showed a slight gradient of particle coverage traveling radially across the surface. This may have been caused by the circular shape of the spray, resulting in a section of the sample lying slightly outside of the spray boundary. Obvious surface features included "coffee-ring effect" geometries to varying degrees depending on solvent composition (Figure 18). These structures were especially prevalent in the 0:1 and 1:3 EtOH:H₂O solutions for 10 and 30 second run times. The 3:1 and 1:0 EtOH:H₂O tests resulted in more frequent, albeit smaller, PSL agglomerations.

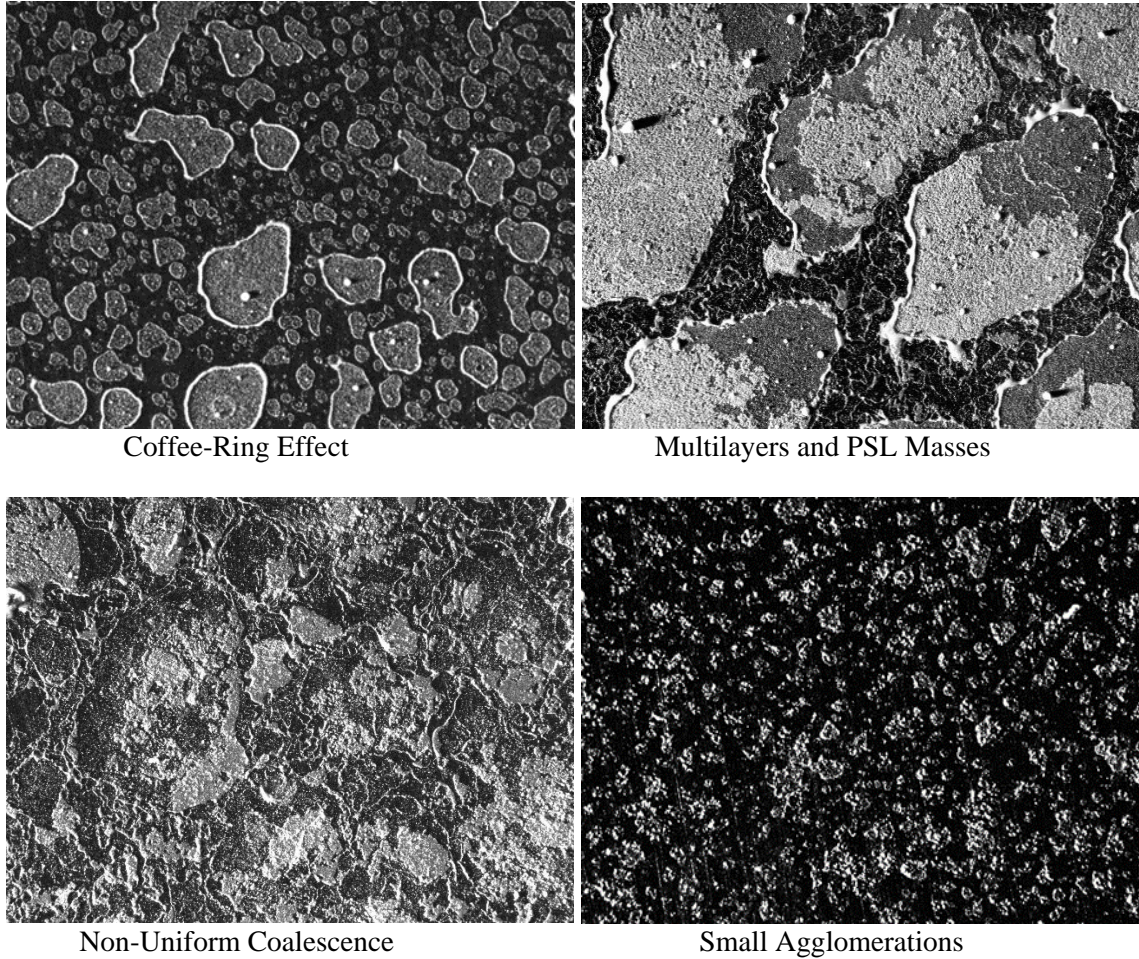


Figure 18. Major PSL contaminant structures observed on polished Al 6061 flat plates. Images were captured at 5x magnification.

Once the initial series of data parameters specified by the DOE was completed, it was determined that further experimental runs were needed to adequately evaluate the influence that N:T pressure had on surface contaminations. Therefore, a second data set was generated. To verify that both of these data sets could be combined, it was important to ascertain how complementary these two data series were. Therefore, an ad-hoc equation (Eq. 1) was generated to differentiate test conditions resulting in a single value numerical value, S , that could be traced through each data series.

$$S=(t*(1-(\%EtOH)/2))/\rho \quad (1)$$

In this equation, t is run time, $\%EtOH$ is the concentration of ethanol in the solution as a weight percentage, and ρ is the particle coverage as an areal percentage. Figure 19 shows the correlation between Data Series 1 and 2 based on the calculated S values. The similarity between the fit lines for each of the data series indicated that the experiments conducted to generate Data Series 1 and 2 could be combined with a nominal increase in the uncertainty.

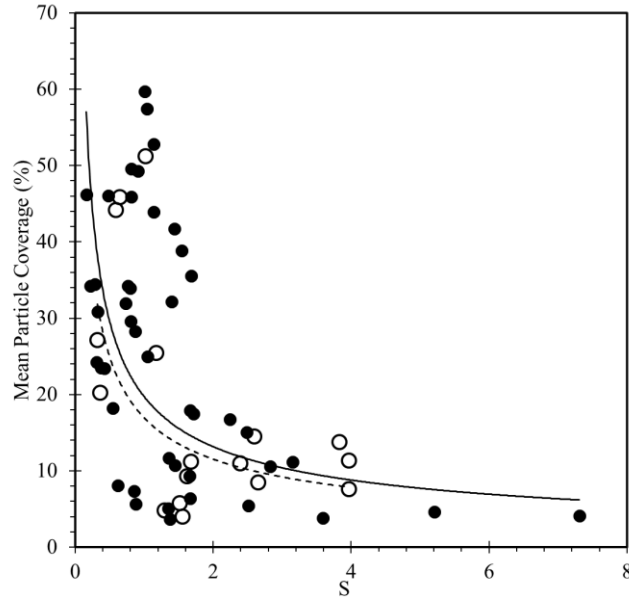


Figure 19. Correlation between contamination data series 1 (filled circles) and 2 (open circles). The fit lines are continuous and dashed for data series 1 and 2, respectively.

Optical micrographs were utilized to both visually and quantitatively ascertain the influence that each input parameter had on surface contamination. Empirical observations performed immediately after each contamination experiment indicated that an increase in both run time and water content resulted in greater surface contamination. To evaluate these observations using the optical micrographs, images were generated which were a compilation of micrographs collected at a single N:T and screen position with run time decreasing from top to bottom, and water content increasing from left to right (N:T of 6 and 12 are shown in Figure 20 and Figure 21, respectively). From the empirical observations, this should result in a progressive increase in PSL contamination from the lower left image to the upper right image.

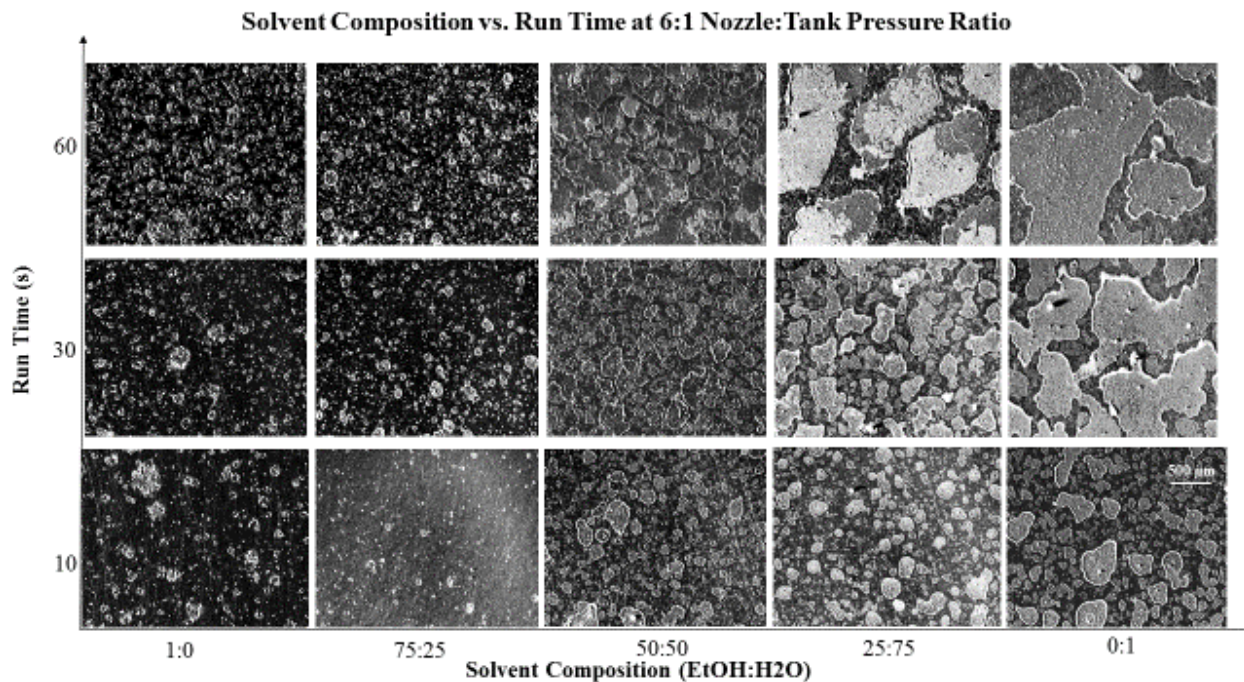


Figure 20. Solvent composition and run time image compilation for contamination experiments conducted at an N:T of 6.

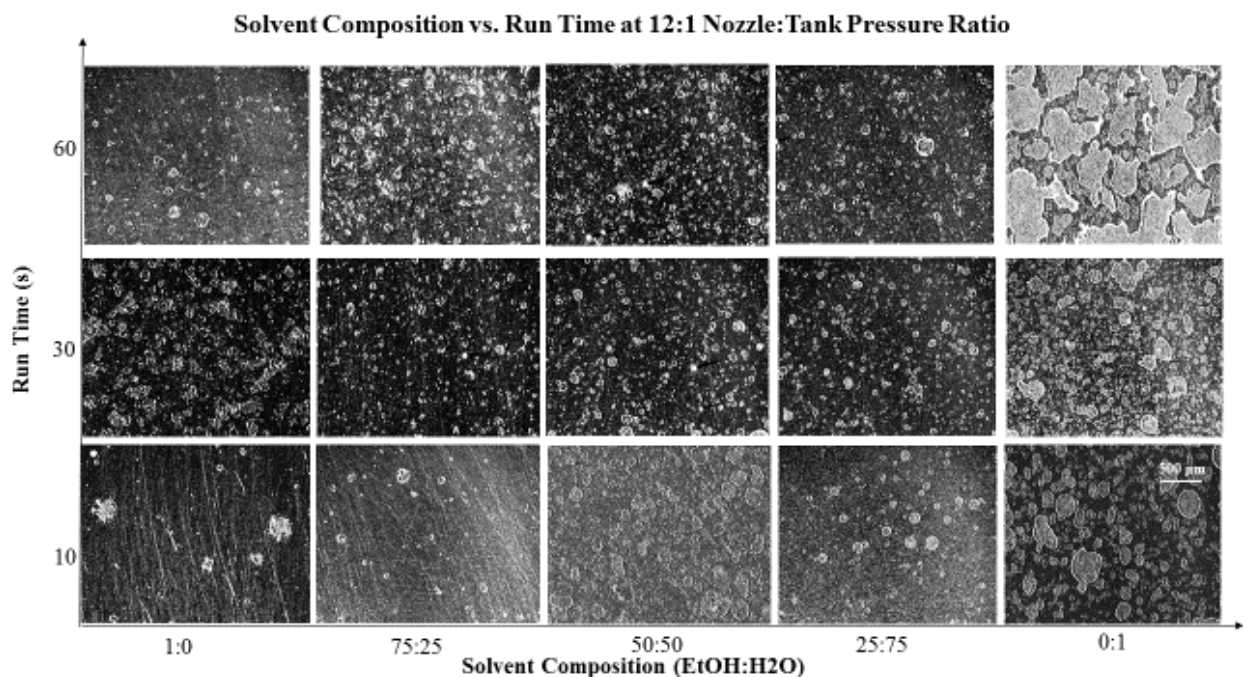


Figure 21. Solvent composition and run time image compilation for contamination experiments conducted at an N:T of 12.

The two trends first identified empirically, that higher run time and greater water solvent content resulted in greater PSL contamination, were also evident in these image compilations. Collectively, these two trends reinforce the idea that the solvent has not been completely removed from the PSLs prior to interacting with the surface of interest, i.e., the cleaning screens. Likewise, the conformation of the PSL deposits observed on the surfaces was indicative of whether or not solvent was present at the time of

surface interaction. In both Figures 20 and 21, the size and frequency of the circular “coffee-ring” deposits increased as the water content and run time increased. Interestingly, at low run times and water content levels, the PSL deposits observed on the contaminated surfaces were present as clustered particles, rather than as independent or monolayer-like deposits. It is unclear whether these clusters were present in the airflow or formed subsequent to surface deposition. Further investigation of this observation is beyond the scope of this work.

Data analysis of the DOE return values was utilized to quantitatively assess the influence that the experimental inputs had on surface contamination. The DOE software was utilized to generate an analysis of variance (ANOVA) report (see Appendix B for the complete report). Upon analysis of the statistical relevance of each experimental input, as well as any cross-terms, solvent composition and N:T were determined to play significant roles in the magnitude of particle contamination. A model was generated with these parameters, as well as run time and air pressure, to predict the particle areal coverage (Figure 22). The coefficient of determination value (R^2 , a measure of how accurately the model reproduces the actual data values) was calculated to be 0.71, which indicated that a reliable model had been generated for this type of multivariate analysis. The calculated probability (p-value) for this model was < 0.001 ; where a p-value ≤ 0.05 is considered to be a reliable indicator of model validity.

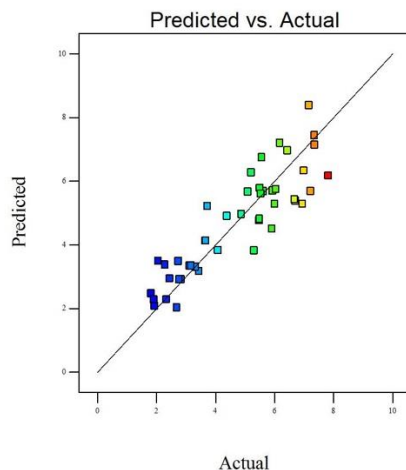


Figure 22. Actual and predicted model results for correlation of % areal coverage.

Utilizing the DOE software, a 3D plot was produced based on the model predictions relating particle areal coverage to run time and solvent composition (Figure 23). Other experimental inputs were kept constant with an N:T of 6:1, a screen position of 1, a substrate orientation of 2, and a central air pressure of 85 psi. The red points in the figure are the actual return values. In agreement to what has already been discussed, it was evident that particle areal coverage increased as water content and run time increased. Interestingly, run time exhibited a greater influence (i.e., a more rapid increase in particle areal coverage) as the water content increased. These results suggested that decreasing water content would reduce the level of wind tunnel surface contamination.

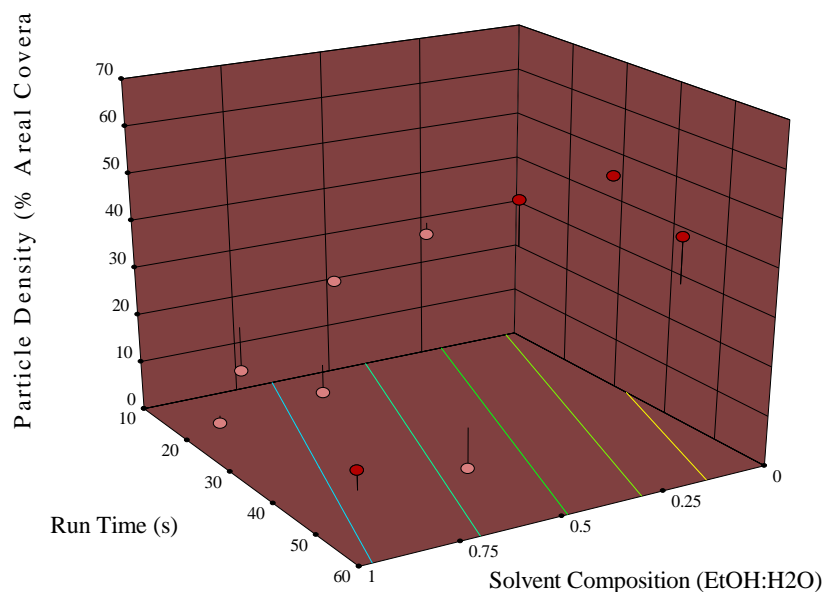


Figure 23. 3D surface of modeled surface contamination as a function of run time and solvent composition.

Dependence of Nozzle and Vessel Pressure Ratio on Surface Contamination

Since solvent volatility was identified as a primary contributor to PSL surface contamination, the N:T was determined to be another potentially meaningful experimental input. Changes to the N:T would change the relative amount of solvent in the airstream. A series of image compilations were generated from optical micrographs to qualitatively evaluate the influence that N:T values had on surface contamination (Figure 24). Regardless of solvent composition, a greater N:T resulted in smaller PSL deposit features. This can be attributed to a lower solvent concentration in airflows generated with greater N:T. This was most evident for experiments conducted with high water content solutions. Lower solvent concentration, as a result of a greater N:T, could result in smaller droplet formation, more rapid solvent evaporation or both. Identification of the relative contribution from these possible changes in the nature of the aerosolized PSL solution was outside the scope of this work. The magnitude of PSL areal coverage also decreased with an increase in the N:T for all of the solvent compositions evaluated.

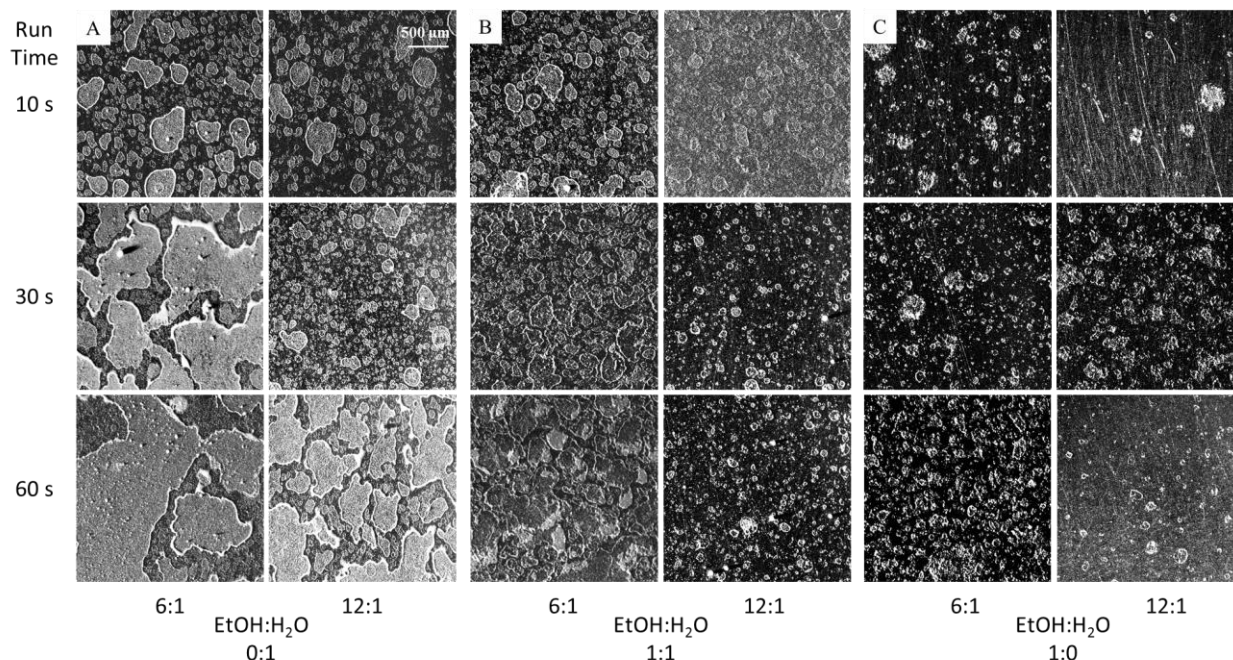


Figure 24. Optical micrographs collected at solvent ratios (EtOH:H₂O) ratios of: (A) 0:1, (B) 1:1, and (C) 1:0). Run times and N:T are indicated in each series of images.

Quantitative assessment of the influence of N:T was performed using the DOE software. Based on the developed model, a 3D plot was generated to compare PSL areal coverage with both N:T pressure ratio and solvent composition (Figure 25). Other experimental inputs were kept constant with a run time of 60 seconds, screen position of 1, a substrate orientation of 2, and a central air pressure of 85 psi. The developed model, represented in this plot, confirmed that similar to ethanol concentration, as N:T increases, PSL areal coverage declines. Similarly, lower water content combined with higher N:T resulted in decreased PSL contamination. The impact N:T had on PSL areal coverage was consistent regardless of solvent composition.

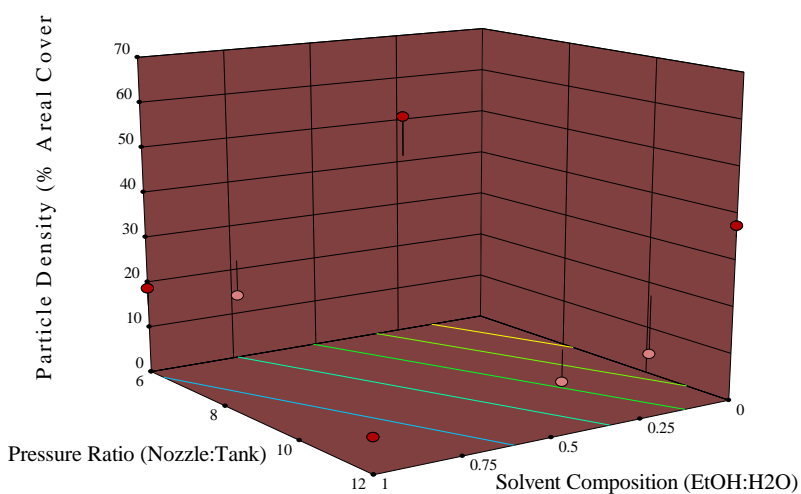


Figure 25. 3D surface of modeled surface contamination as a function of N:T and solvent composition.

Contamination Experiments with Fluorescent Dye Containing Solutions

Collectively, the results from these contamination studies have indicated that two factors contribute toward PSL surface contamination: solvent evaporation rate and the amount of solvent present once the aerosolized droplets interact with the surface of interest. To determine if the solvent evaporation rates were changing significantly prior to surface interaction or if differences in evaporation rate were influencing surface organization behavior, a series of solutions were generated containing Kiton red fluorescent dye. These solutions were generated with identical fluorescent dye concentrations and at EtOH:H₂O ratios of 0:1, 1:1, and 1:0. Each solution was utilized in the contamination rig assembly, to ascertain the level of surface contamination by the fluorescent dye. Once the contamination experiment was completed, the contaminated surface was allowed to dry overnight and the same volume of water was utilized on each sample to dissolve any deposited dye. To qualitatively assess the amount of dye deposited on each surface, this solution was placed in a test tube and illuminated with UV light (Figure 26).

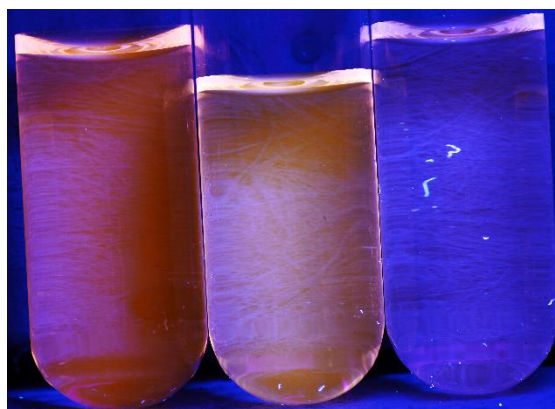


Figure 26. Rinse water under UV illumination from contamination experiment surfaces exposed to spray by solvents containing Kiton red. EtOH:H₂O ratios were: (left) 0:1, (middle) 1:1, (right) 1:0.

The difference in luminescence between the samples was indicative of the relative quantities of Kiton red dye that interacted with the contaminated substrates through a liquid droplet. Based on Figure 26, it was evident that the 0:1 EtOH:H₂O solution resulted in the greatest level of dye deposition. Conversely, the collected rinse water from the contamination surface generated from the 1:0 EtOH:H₂O solution appeared to have negligible Kiton red dye. This was further verification that both ethanol droplets evaporated and water droplets did not prior to reaching the substrate. These experiments confirmed that PSL coverage on the aluminum substrates was strongly affected by solution composition and as solvent water content decreased, surface contamination decreased due to the presence of less solvent at the time of surface interaction.

Verification Experiments on Stainless Steel Screen Samples

To confirm that the results obtained on flat aluminum surfaces were translatable to the cleaning screens, a series of experiments were conducted that were designed to result in either high or low levels of contamination. Two screen samples were evaluated in the contamination rig using solvent compositions that were either 0:1 or 1:0 EtOH:H₂O. The remaining experimental inputs were kept constant with a run time of 60 seconds, a N:T of 6:1, a screen position 1, and a central air pressure of 70 psi. The screens were photographed and compared to an untested screen sample (Figure 27).

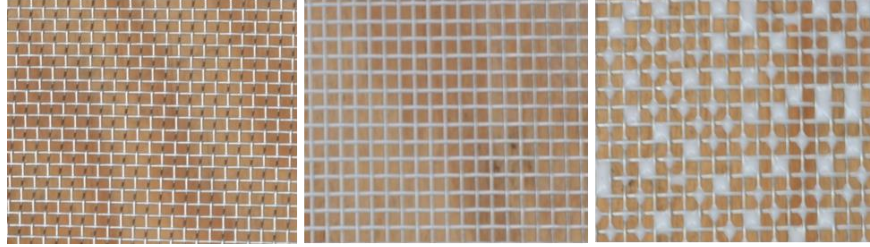


Figure 27. (A) Uncontaminated stainless steel screen. (B) A stainless steel screen exposed to 1:0 (EtOH:H₂O) PSL solution spray. (C) A stainless steel screen exposed to 0:1 (EtOH:H₂O) PSL solution spray.

Based on these images, it was obvious that after 60 seconds, the screen exposed to the 0:1 EtOH:H₂O solution was contaminated to a much greater level than the screen exposed to the 1:0 EtOH:H₂O solution. In fact, so much solvent was present at the time of droplet interaction with the screen surface that liquid droplets filled many of the open regions of the screen. Beyond enabling deposition of large quantities of PSLs on the screen surface, this filled space could restrict airflow and lower the screens ability to reduce velocity variation within the airflow. Although significantly less than the 0:1 EtOH:H₂O case, the screen contaminated with 1:0 EtOH:H₂O exhibited a slight coating of PSLs compared to the uncontaminated screen, observed as a reduction in reflectivity after the contamination experiment was completed.

Thermodynamic Analysis of Liquid Droplet Evaporation

To gain an understanding of the thermodynamic behavior the droplets once released from the ultrasonic nozzle, solvent diffusion calculations were performed. A differential equation was utilized to determine the time required for a liquid droplet of a specified initial diameter to evaporate under known environmental conditions (Eq. 2).¹⁸

$$\frac{dD}{dt} = -\frac{4MD_v\Delta p}{D\rho RT} \left(1 + 0.276R_e^{\frac{1}{2}}S_c^{\frac{1}{3}} \right) \quad (2)$$

In this equation, D is the diameter of the droplet, M is the molecular weight of the liquid, D_v is the diffusion coefficient for the liquid, Δp is the difference between vapor pressure near the drop and that in the ambient atmosphere, ρ is the density of the liquid, R is the gas constant (8.314 J mol⁻¹ K⁻¹), T is the absolute temperature (in K) in the vapor film surrounding the liquid droplet, Re is the Reynolds' number, and Sc is the Schmidt number. Assuming there is no transfer of energy between the surrounding air and the particle creating viscous motion, Re becomes zero and the change in diameter with respect to time simplifies to Eq. 3.

$$\frac{dD}{dt} = -\frac{4MD_v\Delta p}{D\rho RT} \quad (3)$$

A Mathematica code was written to solve this differential equation and a model was generated that predicted the time required for a liquid droplet of 4 μm to evaporate (Figure 28, see Appendix C for the Mathematica code). In this model, it was assumed the temperature of the vapor film surrounding the droplet was at equilibrium temperature with the ambient air, in this case, 25 °C. Using various sources, values for D_v, Δp, and ρ were either found or calculated.¹⁹⁻²¹ Raoult's law was utilized to calculate the partial pressures of the EtOH:H₂O mixtures. Additionally, a change in the relative humidity (RH) was included to account for measured differences in RH values immediately beyond the nozzle, assumed to be

100% for droplets containing water, to a value of 85% measured at the first screen position. See Appendix D for details of these measurements.

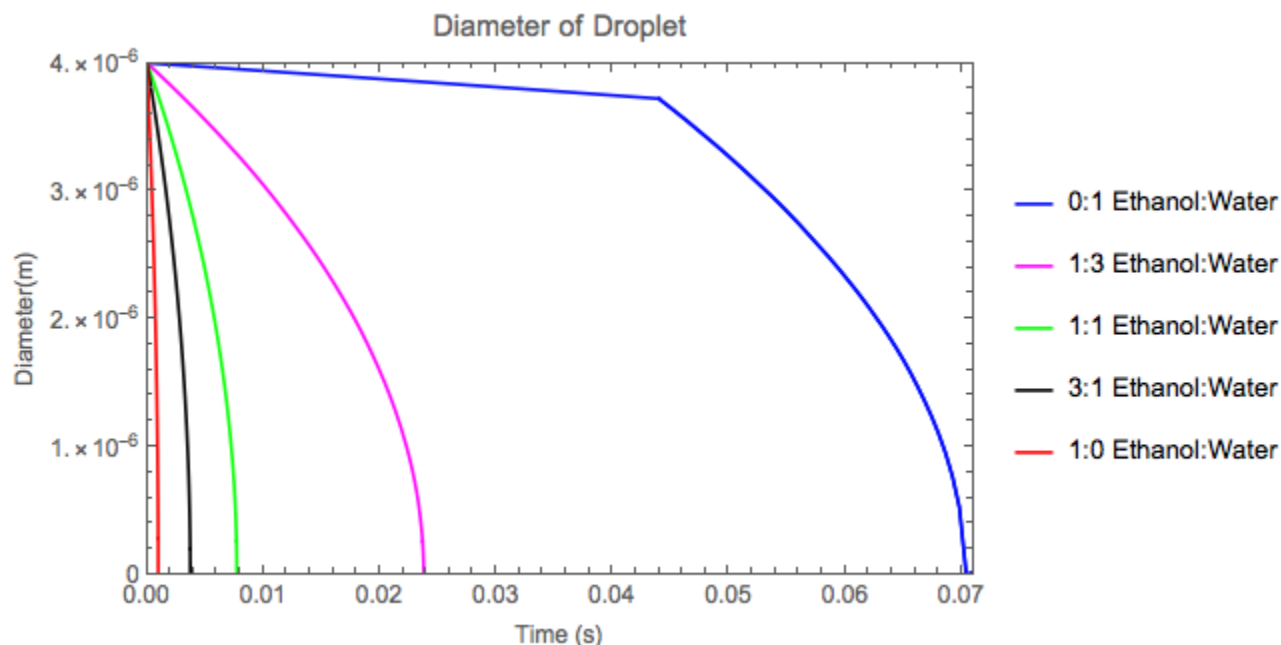


Figure 28. The time dependence for a 4 μm droplet of different solvent composition to evaporate.

Based on the model results, there was an obvious trend in evaporation behavior. In agreement with what was determined experimentally, droplets with greater ethanol concentration evaporated more rapidly than those with higher water concentration. For example, a droplet comprised of 1:0 EtOH:H₂O was calculated to evaporate approximately seven times and thirty times faster than a droplet of the same size comprised of 1:1 and 0:1 EtOH:H₂O, respectively. Using the calculated rate of evaporation and the airspeed/distance relationship measured in the contamination rig (see Appendix D), it was possible to calculate the distance, *d*, at which each droplet would have completely evaporated (Table 4).

Table 4. Calculated distance required for complete solvent evaporation.

EtOH:H ₂ O Ratio	Evaporation Time, ms	<i>d</i> , inches
0:1	70.5	20.6
1:3	24.0	8.9
1:1	7.3	3.2
3:1	3.7	1.7
1:0	0.9	0.4

Although the theoretical distance traveled for complete solvent evaporation was significantly less than what was observed experimentally, for example the first screen position was approximately 22 in from the nozzle and there was clear liquid deposition at this position even at a EtOH:H₂O ratio of 1:1, the overall trend was consistent. Therefore, the model developed here can be considered useful as a starting point for considering different solvent compositions including different EtOH:H₂O ratios as well as completely new solvent components. Since the model was built on basic principles of diffusion using physical constants as inputs, it can be readily adapted to new solvent compositions.

Conclusion and Outlook

Solvent evaporation was determined to be critical regarding the tenacity of PSLs to adhere to incident surfaces. Since solvent-based seeding of airflows with PSLs has been broadly utilized for flow visualization, the work described here may enable this approach to flow visualization to continue to be utilized with little modification to experimental configuration. Changes in solvent composition and the relative amount of solvent-laden air mass in the seeded airflow should enable a dramatic reduction in facility contamination. Although the substrates investigated in this work were limited to metallic surfaces, the capillary forces involved in PSL-substrate interactions when solvent is present can be readily translated to plastic and ceramic surfaces. Thus, experimental modification to reduce contamination of metallic surfaces should be beneficial to other material surfaces as well. Similarly, as substrate roughness was identified as an important factor in surface contamination, reducing substrate topographical features, if possible, would also reduce surface contamination. Further, the solvent evaporation model developed in this work was designed such that it could be modified to accommodate different solvent compositions extending its capabilities.

References

1. Adrian, R.; Westerweel, J., *Particle Image Velocimetry*. Cambridge University Press: New York, 2011.
2. Raffel, M.; Willert, C.; Kompenhans, J., *Particle Image Velocimetry: A Practical Guide (Experimental Fluid Mechanics)*. 2nd Edition ed.; Springer: Berlin, Germany, 2007; p 448.
3. Tiemsin, P.; Wohl, C. J. Refined Synthesis and Characterization of Controlled Diameter, Narrow Size Distribution Microparticles for Aerospace Research Applications. National Aeronautics and Space Administration, 2012, TM-2012-217591.
4. Melling, A., Tracer Particles and Seeding for Particle Image Velocimetry. *Meas. Sci. Technol.* **1997**, 8, pp 1406-1416.
5. Meyers, J. F. In *Generation of Particles and Seeding*, von Karman Institute for Fluid Dynamics, NASA Langley Research Center, Hampton, VA, June 10-14.
6. Danehy, P.; Tiemsin, P.; Wohl, C.; Verkamp, M.; Lowe, T.; Maesto, P.; Byun, G.; Simpson, R. Fluorescence Doped Particles for Simultaneous Temperature and Velocity Imaging. National Aeronautics and Space Administration, 2012, TM-2012-217768.
7. Lowe, T.; Maesto, P.; Byun, G.; Simpson, R.; Danehy, P.; Tiemsin, P.; Wohl, C., Laser Velocimetry with Fluorescent Dye-doped Polystyrene Microspheres. *Optics Lett.* **2013**, 38 (8), pp 1197-1199.
8. Wohl, C. J.; Kiefer, J. M.; Tiemsin, P. I.; Maisto, P. M. F.; Lowe, K. T.; Danehy, P. M., Synthesis of Fluorophore-doped Polystyrene Microspheres: Optimization through Design of Experiments Methodologies. *Macromolecules* **2015**, p manuscript in preparation.
9. Closed Return Wind Tunnel. <https://www.grc.nasa.gov/www/K-12/airplane/tuncrret.html> (accessed February 9, 2018).
10. Smith, J. R.; Banerjee, A., New Approach to Calculation of Total Energies of Solids with Defects: Surface-Energy Anisotropies. *Physical Review Letters* **1987**, 59 (21), pp 2451-2454.
11. Li, Y.; Yu, J.; Li, W.; Fan, G.; Yang, L.; Li, F., The promotional effect of surface defects on the catalytic performance of supported nickel-based catalysts *Physical Chemistry Chemical Physics* **2016**, 18, pp 6548-6558.
12. Ferguson, A.; Caffrey, I. T.; Backes, C.; Coleman, J. N.; Bergin, S. D., Differentiating Defect and Basal Plane Contributions to the Surface Energy of Graphite Using Inverse Gas Chromatography. *Chem. Mater.* **2016**, 28 (17), pp 6355-6366.
13. Bueno, H. The Critical Surface Tension of 316L Stainless Steel. thesis, San Jose State University, San Jose, 2005.

14. Anyfantakis, M.; Baigl, D., Manipulating the Coffee-Ring Effect: Interactions at Work. *ChemPhysChem* **2015**, *16*, pp 2726-2734.
15. Hu, H.; Larson, R. G., Marangoni Effect Reverses Coffee-Ring Depositions. *J. Phys. Chem. B* **2006**, *110* (14), pp 7090-7094.
16. Yunker, P. J.; Still, T.; Lohr, M. A.; Yodh, A. G., Suppression of the coffee-ring effect by shape-dependent capillary interactions. *Nature* **2011**, *476*, pp 308-311.
17. *Particle Adhesion and Removal*. Mittal, K. L.; Jaiswal, R., Eds. Wiley-Scrivener: New York, 2015.
18. Holterman, H. J., *Kinetics and Evaporation of Water Drops in Air*. IMAG: 2003.
19. Martinez, I. Mass Diffusivity Data. <http://webserver.dmt.upm.es/~isidoro/dat1/Mass%20diffusivity%20data.pdf> (accessed February 9, 2018).
20. Shallcross, D., *Handbook of Psychrometric Charts*. Springer: Netherlands, 1997; p 317.
21. *Handbook of Chemistry and Physics*. 98th Edition ed.; Rumble, J. R., Ed. CRC Press: Boca Raton, FL United States of America, 2017.

Appendix A: Image Analysis and Verification

Image Analysis Methodology

Following microscopy, Z-Stack Acquisition images were analyzed using ImageJ (Image Processing and Analysis in Java) software. After opening the specific file, the threshold of each image was adjusting by changing the settings of the maximum, minimum, brightness, and contrast as shown in Figures A1 and 16. The image's pixel size was then calibrated by identifying the known distance and unit of length (e.g. 20 μm), enabling the software to measure specific aspects of the microstructure (Figure A1).

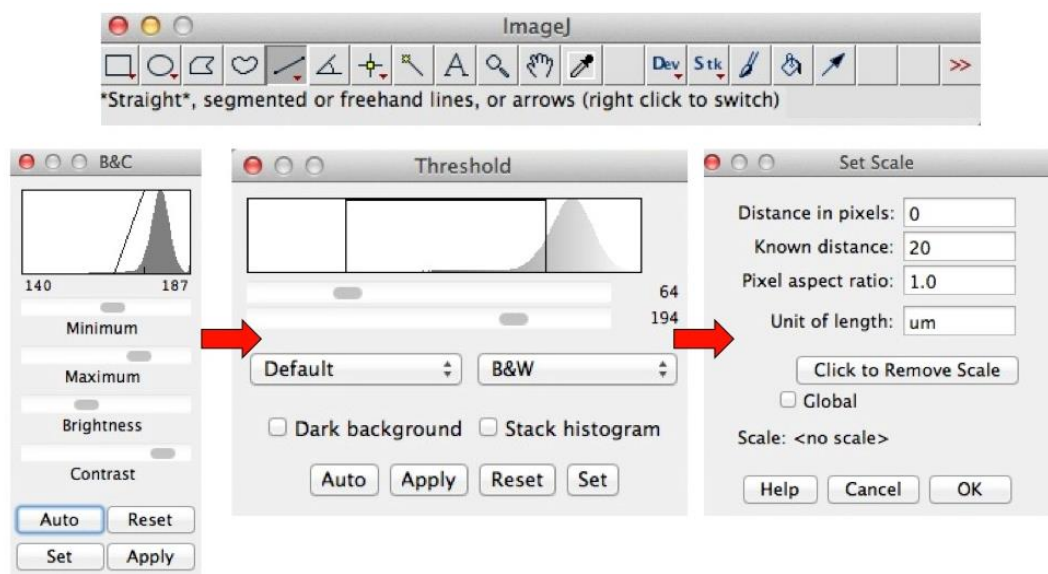


Figure A1. ImageJ thresholding and scale functions.

Once the particles exhibited a clear, visible contrast to the background, the image was altered using the binary function (Figure A2). This further differentiated the PSL from the background. Although the images did originally exhibit some contrast in the initial confocal image, a binary image was necessary for the software to identify pixels as particles (black) against the background (white). A mapped image was created following the “Analyze Particles” function displayed in Figure A3. The image on the far right of Figure A2 shows the outlines of the particles and numbers each particle displayed in the “Results” function.

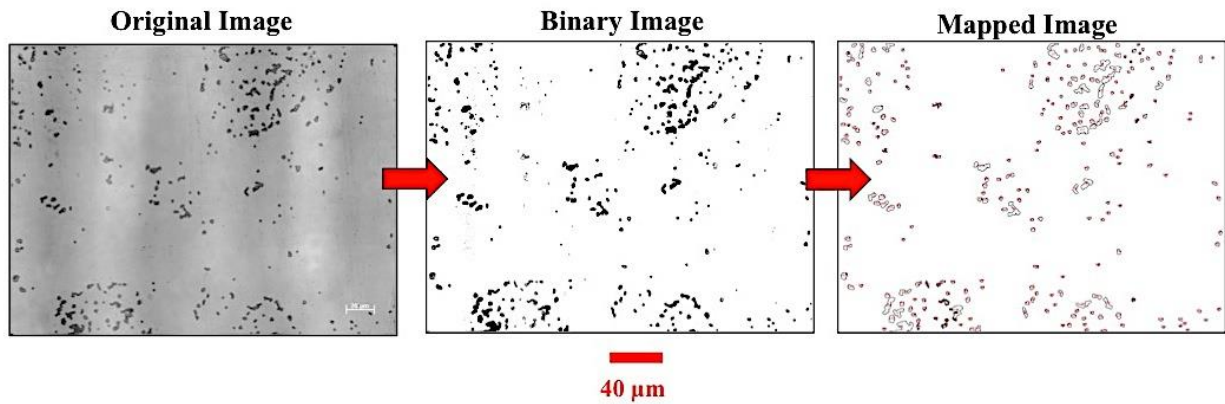


Figure A2. Original, binary, and particle analysis mapped images in ImageJ.

Using the “Analyze Particles” function, the particles in each image were evaluated. For the most accurate results, the size of the particles in the function was altered according to the magnification used to capture the image. For example, the initial particle size was adjusted to $1.75 \mu\text{m}^2$ for 50x images which prevented small non-PSL particulate contamination or metallic features from skewing the results. This study utilized the summary function’s data of particulate population, average size, and area fraction (the percentage of space the particles utilize). However, the results function has the capability to output statistics for each individual particle, providing an exhaustive study of particle size and distribution for future research. An example of the data output for one image is presented in Figure A3 through analysis of each individual particles and the representative average of the entire area.

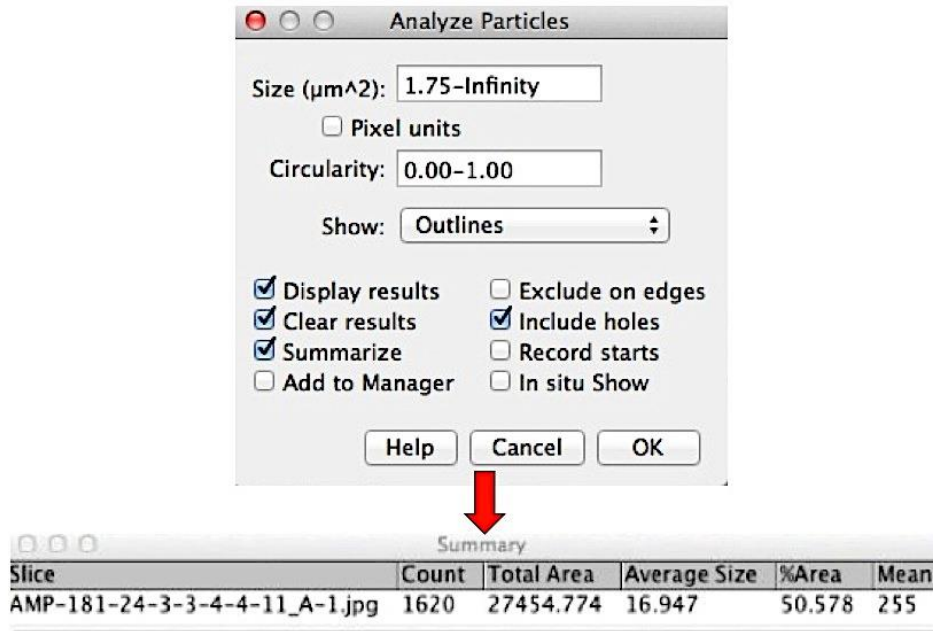


Figure A3. Particle data computed for count, size, and %area with ImageJ.

The calculations of each sample’s ImageJ results were compared to determine any trends from region to region and sample to sample. Area fractions ranged from approximately 1 to 99 %, measuring the ratio between particles and the surrounding background. Qualitative and ImageJ data analysis of imaging was used to evaluate the mechanisms of PSL adhesion in order to offer greater insight into improving the synthesis of PSL microspheres to mitigate particle contamination of wind tunnel screens.

Image Analysis Validation

A validation of ImageJ % area accuracy was completed by performing two tests. One was performed with a 5 in x 5 in square image that consisted of 25 1 in x 1 in squares touching. Figure A4 represents the lack of accuracy in ImageJ's approach to counting, sizing, and determining the area of the squares. The figure contains an example of the squares analysis and the plot of ImageJ's accuracy. The image on the left actually contains 48% coverage by the squares, but ImageJ considers the entire image as a single square or "particle." This test demonstrates the similar effects of ImageJ analysis with particle agglomerations and multilayers as ImageJ fails to account for individual particles that are connected. The first two data plots, however, contained squares that were not connected and produced highly accurate results with ImageJ analysis.

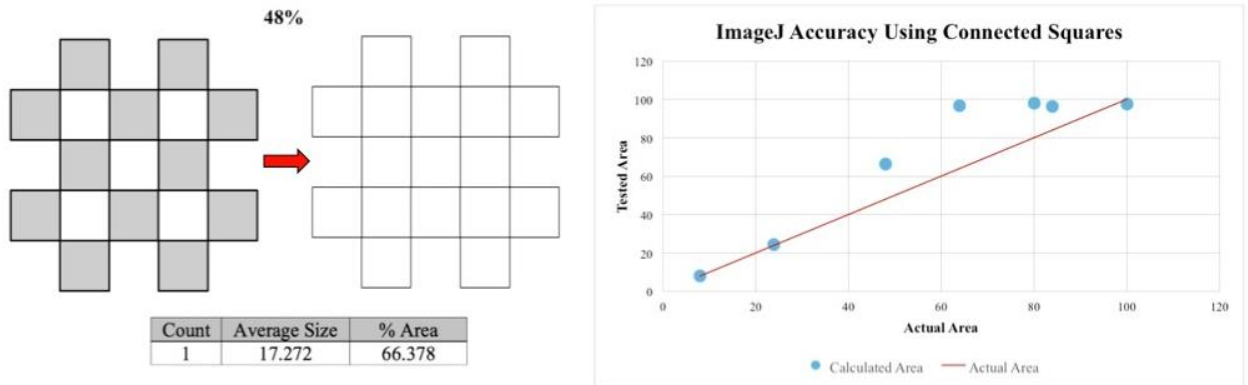


Figure A4. ImageJ accuracy test with connected squares.

A second test was performed with 0.25 in x 0.25 in squares within a 5 in x 5 in square that could contain 400 of the small squares connected. The small squares, however, were spaced apart. Figure A5 shows one of the trials on the left with an actual 9.25% coverage and 35 squares. ImageJ correctly counted the number of small squares and produced values close to the actual size of 0.0625 in² and 9.25% area. On the right of the figure, a plot of ImageJ's accuracy is displayed. When particles are not touching, ImageJ performs best, especially at lower values.

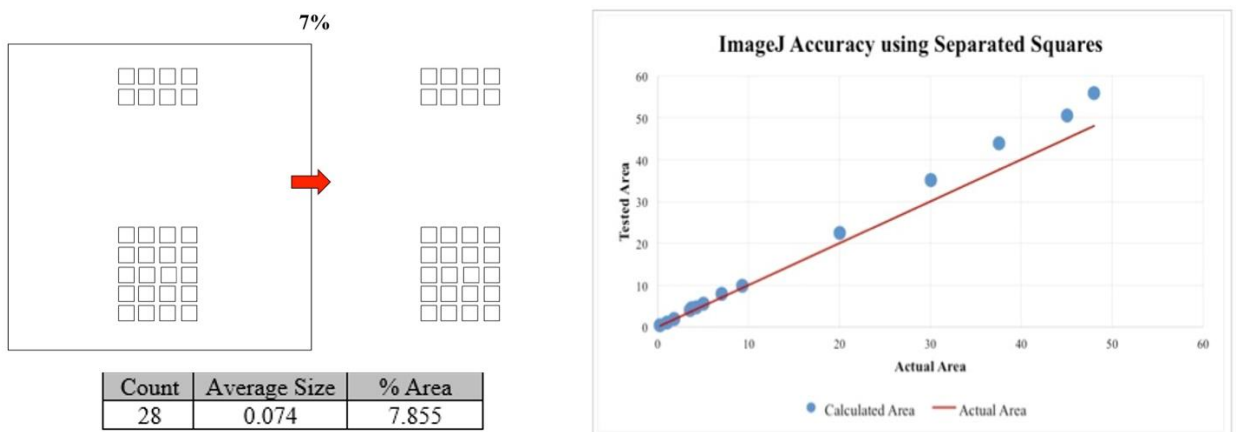


Figure A5. ImageJ accuracy test with separated squares.

Appendix B: Design of Experiments Data and Statistical Analysis

Data Series 1

(EtOH:H ₂ O)	Run Time (s)	Pressure Ratio (Nozzle:Tank)	Screen Position	Substrate Orientation	Central Air Pressure (PSI)	Mean Particle Coverage (%)
0:1	10	6	1	1	70	34.5
0:1	60	6	3	1	70	59.7
0:1	40	6	3	5	85	49.6
0:1	60	6	1	5	70	52.8
0:1	60	8	1	9	85	41.7
0:1	24	8	1	9	85	29.6
0:1	26	8	3	9	70	34.2
0:1	10	8	3	1	85	30.9
0:1	60	12	3	9	85	35.6
0:1	10	12	1	9	85	18.2
0:1	60	12	1	9	70	57.4
0:1	50	12	1	1	85	44.0
0:1	60	12	1	5	85	38.8
0:1	10	12	3	5	70	23.5
25:75	10	6	3	9	85	23.5
25:75	30	12	3	1	70	25.0
50:50	30	6	1	1	85	46.1
50:50	50	6	1	9	85	45.9
50:50	10	8	1	5	85	46.2
50:50	60	8	3	5	70	32.2
50:50	60	8	3	5	70	49.3
50:50	10	8	1	5	85	34.2
50:50	30	8	1	5	70	32.0
50:50	36	8	1	9	70	33.9
50:50	10	12	1	1	70	24.3
75:25	40	6	3	5	85	28.3
75:25	60	8	3	1	85	16.7
75:25	60	8	3	1	85	15.1
75:25	55	12	1	9	85	7.5
75:25	25	12	3	5	85	10.0
75:25	38	12	1	1	85	4.6
75:25	10	12	3	9	70	7.3
75:25	25	12	3	5	85	9.3
1:0	21	6	3	1	70	6.4
1:0	10	6	1	9	70	8.1
1:0	10	6	3	5	70	5.7
1:0	60	6	1	5	85	18.0
1:0	27	8	3	9	85	5.4
1:0	60	8	1	1	70	17.5
1:0	60	6	3	9	70	10.6
1:0	27	8	3	9	85	3.8
1:0	15	8	1	1	85	5.1
1:0	10	12	1	1	85	3.6
1:0	60	12	3	1	70	4.1
1:0	31	12	1	5	70	11.7

Data Series 2

(EtOH:H ₂ O)	Run Time (s)	Pressure Ratio (Nozzle:Tank)	Screen Position	Substrate Orientation	Central Air Pressure (PSI)	Mean Particle Coverage (%)
0:1	30	6	1	5	85	45.8
0:1	30	12	1	5	85	25.4
25:75	10	6	1	5	85	27.1
25:75	30	6	1	5	85	44.2
25:75	60	6	1	5	85	51.2
25:75	10	12	1	5	85	5.8
25:75	30	12	1	5	85	10.9
25:75	60	12	1	5	85	13.7
50:50	10	6	1	5	85	20.2
50:50	30	12	1	5	85	8.5
50:50	60	12	1	5	85	11.3
75:25	10	6	1	5	85	4.0
75:25	30	6	1	5	85	11.2
75:25	60	6	1	5	85	14.4
75:25	10	12	1	5	85	4.8
1:0	30	6	1	5	85	9.2
1:0	60	12	1	5	85	7.6

Anova Report

Source	Sum of Squares	df	Mean Square	F Value	p-value (Prob>F)
Model	138.21	4	34.55	35.28	8.08×10 ⁻¹⁵
A-Solvent Composition	106.68	1	106.6	108.9	7.65×10 ⁻¹⁵
B-Run Time	10.809	1	10.80	11.03	1.56×10 ⁻³
C-Pressure Ratio	22.717	1	22.71	23.19	1.12×10 ⁻⁵
E-Wall Pressure	4.3225	1	4.322	4.413	0.040
Residual	55.819	57	0.979		
Lack of Fit	54.008	52	1.038	2.866	0.119
Pure Error	1.8115	5	0.362		
Cor total	194.03	61			

The Model F-value of 35.28 implies the model is significant. There is only a 0.01% chance that an F-value this large could occur due to noise.

Values of "Prob > F" less than 0.0500 indicate model terms are significant. In this case A, B, C, F are significant model terms.

The "Lack of Fit F-value" of 2.87 implies the Lack of Fit is not significant relative to the pure error. There is a 11.93% chance that a "Lack of Fit F-value" this large could occur due to noise.

Std. Dev.	0.99	R-Squared	0.71
Mean	4.53	Adj R-Squared	0.69
C.V. %	21.9	Pred R-Squared	0.66
PRESS	65.3	Adeq Precision	23.2

The "Pred R-Squared" of 0.66 is in reasonable agreement with the "Adj R-Squared" of 0.69; i.e. the difference is less than 0.2.

"Adeq Precision" measures the signal to noise ratio. A ratio greater than 4 is desirable. Your ratio of 23.152 indicates an adequate signal. This model can be used to navigate the design space.

Factor	Coefficient Estimate	df	Standard Error	95% CI		VIF
				Low	High	
Intercept	4.5979	1	0.1348	4.328	4.868	
A-Solvent Comp	-1.754	1	0.1680	-2.090	-1.418	1.009
B-Run Time	0.5221	1	0.1572	0.207	0.837	1.004
C-Pressure Ratio	-0.693	1	0.1440	-0.982	-0.405	1.008
F-Wall Pressure	-0.283	1	0.1348	-0.553	-0.013	1.005

Appendix C: Mathematica Code for Determination of Droplet Evaporation Rate

NOTE: Not all cases have been included for brevity.

Rate of Change of Droplet Diameter as a result of Evaporation;

```

M= Molecular weight of evaporating liquid;
  (Water-- .018 kgmol-1);
  (Ethanol-- .04606844 kg-1mol);
Dv= average diffusion coefficient for vapor molecules in the saturated film
around drop (m2 s-1);
  (Water-- 24 * 10-6);
  (Ethanol-- 11 * 10-6);
ρ= density of liquid (kgm-3);
  (Water-- 1000 kgm-3)
  (Ethanol-- 789 kgm-3)
Tf= average absolute temperature in that film (K);
  (F→C= (F - 32) * 5/9);
  (C→K= C+273.15);
Δp= Pdrop - Pair = difference between the vapor pressure near the drop and that in
the ambient atmosphere (Pa = kgm-1 s-2);
  (Pdropwater = CHECK TABLE VALUES);
  (Pdropethanol = CHECK ETHANOL PRESSURE TABLE);
  (Pairwater = CHECK PSYCHROMETRIC CHART);
  (Pairethanol = 0);
  (Pa= 133.322368*torr);
  (Pa= 33.8639 * PinHg * 102);
R= gas constant (=8.3144 Jmol-1 K-1 = kgm2 s-2 K-1 mol-1);
d=Diameter of a spherical drop (m);
v=0 velocity of drop relative to surrounding air (ms);
ρa= air density at temperature Tf;
νa= air viscosity at temperature Tf;
K= evaporation rate;

```

EVAPORATION OF 0:1 ETHANOL:WATER DROPLET [077F=25C=298.15K, & 100% RH];;

```

ClearAll[Local]
M = .018 ;
Dv = 24 * 10-6;
Δp = 3167.204 - 3132.41;
d0 = 4 * 10-6;
ρ = 1000;
R = 8.3144;
Tf = 298.15;

```

Here we are assuming the droplets are traveling at the same speed as the airflow, so Re from the master equation = 0. Therefore, the rate of decrease of the diameter d is:

$$d' = \frac{-(4 M * Dv)}{d * \rho * R * Tf} * \Delta p;$$

$$a = -(4 M * Dv) * \Delta p;$$


$$b = \rho * R * Tf;$$

This line is used to solve the differential equation:

```

diam = NDSolve[{d'[t] == a/b, d[0] == 4 * 10-6}, d, {t, 0.0, 2}, MaxSteps -> 2 000 000];

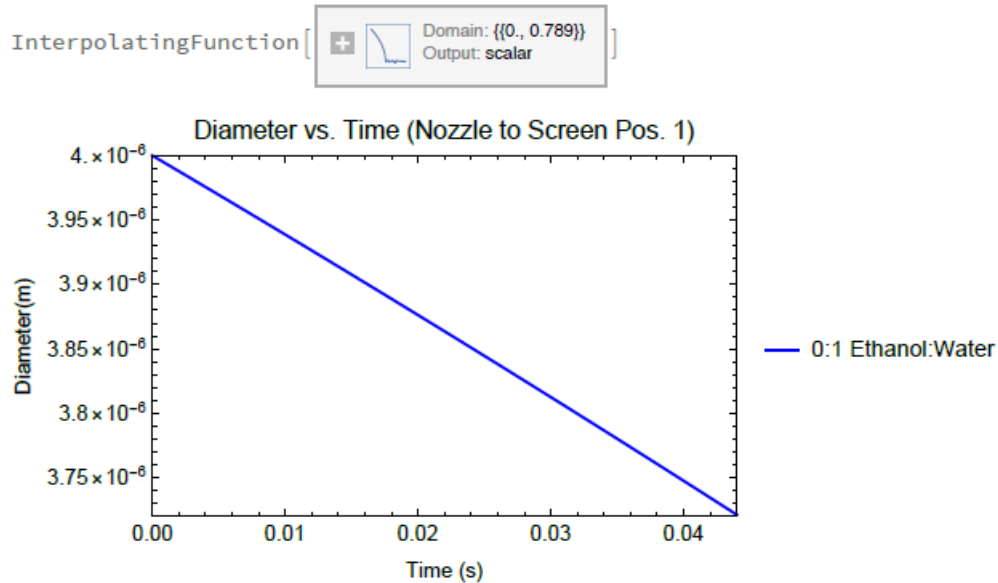
```

 **NDSolve:** At t == 0.7893593561976916', step size is effectively zero; singularity or stiff system suspected.

```

solution = diam[[1, 1, 2]]
plot1a = Plot[solution[t], {t, 0., 0.044},
  PlotLegends → LineLegend[{{Blue}}, {"0:1 Ethanol:Water"}], PlotStyle → Blue,
  PlotLabel → "Diameter vs. Time (Nozzle to Screen Pos. 1)",
  PlotRange → {{0, 0.044}, {3.72 * 10-6, 4.0 * 10-6}},
  Frame → {True, True, True, True}, FrameLabel → {"Time (s)", "Diameter (m)"},
  FrameTicks → Automatic, BaseStyle → {FontSize → 12}]

```



This plot shows us that in the time it takes for the droplet to reach screen position 1 exposed to 100% relative humidity (RH), the droplet diameter has reached $3.72 \mu\text{m}$, a decrease of $0.28 \mu\text{m}$.

Using the air speed of 2500 ft/min or 500in/s, we then continue the calculation at 85% RH, starting from the diameter at screen position 1 until it reaches screen position 3 (40" from the nozzle).


```

ClearAll[Local]
M = .018 ;
Dv = 24 * 10-6;
Δp = 3167.204 - 2793.77;
d0 = 3.72 * 10-6;
ρ = 1000;
R = 8.3144;
Tf = 298.15;
d' =  $\frac{-(4 M * Dv)}{D * \rho * R * Tf} * \Delta p$ ;
a =  $-(4 M * Dv) * \Delta p$ ;
b =  $\rho * R * Tf$ ;
diam =
NDSolve[{d'[t] ==  $\frac{a}{b}$ , d[0] == 3.72 * 10-6}, d, {t, 0.0, 2}, MaxSteps -> 2000000];


```

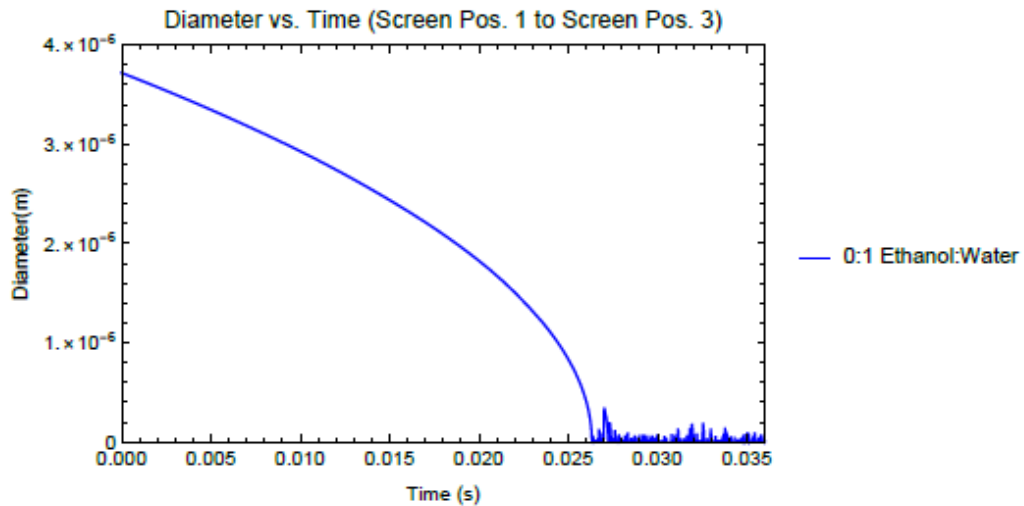
NDSolve: At t == 0.05762761888130248, step size is effectively zero; singularity or stiff system suspected.

```

solution = diam[[1, 1, 2]]
plot1b = Plot[solution[t], {t, 0.0, 0.036},
  PlotLegends -> LineLegend[{Blue}, {"0:1 Ethanol:Water"}], PlotStyle -> Blue,
  PlotLabel -> "Diameter vs. Time (Screen Pos. 1 to Screen Pos. 3)",
  AxesLabel -> {"Time (s)", "Diameter(m)"}, PlotRange -> {{0, 0.036}, {0, 4.0 * 10-6}},
  Frame -> {True, True, True, True}, FrameLabel -> {"Time (s)", "Diameter(m)"},
  FrameTicks -> Automatic, BaseStyle -> {FontSize -> 12}]

```

InterpolatingFunction[ Domain: {{0., 0.0576}} Output: scalar]



This plot shows us that after screen position 1 at 85% RH, the droplet will have fully evaporated after 0.026 s, which corresponds to full evaporation before reaching screen 3. The spikes are due to an error in the equation after the diameter has reached 0 μm .

```

ClearAll[Local]
M = .018 ;
Dv = 24 * 10-6;
Δp = 3167.204 - 2793.77;
d0 = 3.72 * 10-6;
ρ = 1000;
R = 8.3144;
Tf = 298.15;
d' =  $\frac{-(4 M * Dv)}{D * \rho * R * Tf} * \Delta p$ ;
a =  $-(4 M * Dv) * \Delta p$ ;
b =  $\rho * R * Tf$ ;
diam =
NDSolve[{{d'[t] ==  $\frac{a/b}{d[t]}$ , d[0] == 3.72 * 10-6}, d, {t, 0.0, 2}, MaxSteps -> 2 000 000];


```

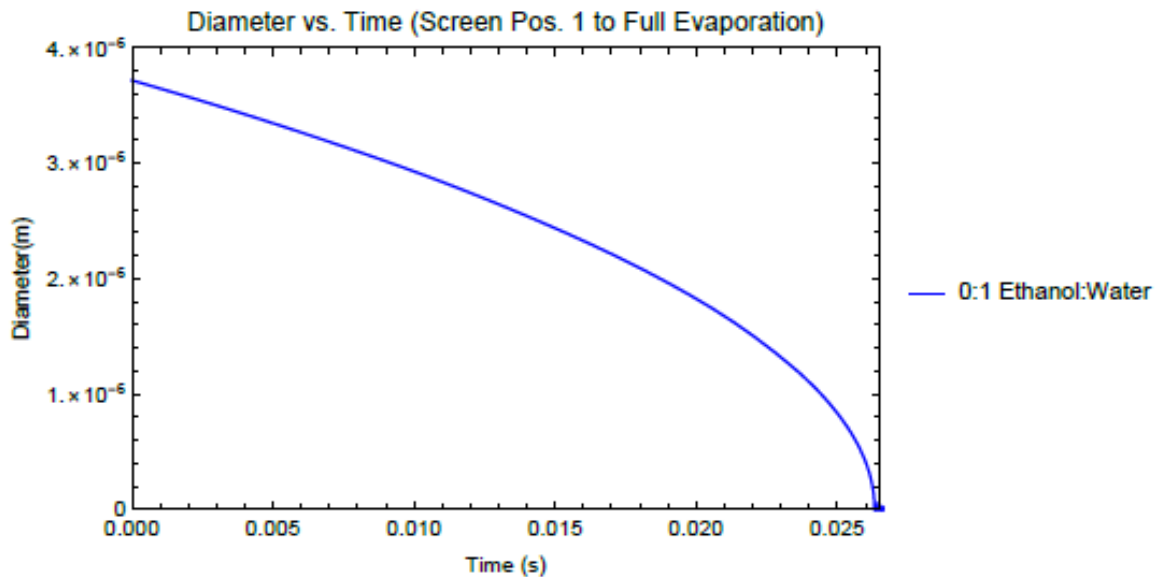
 **NDSolve:** At t == 0.05762761888130248, step size is effectively zero; singularity or stiff system suspected.

```

solution = diam[[1, 1, 2]]
plotlc = Plot[solution[t], {t, 0.0, 0.036},
  PlotLegends → LineLegend[{Blue}, {"0:1 Ethanol:Water"}], PlotStyle → Blue,
  PlotLabel → "Diameter vs. Time (Screen Pos. 1 to Full Evaporation)",
  AxesLabel → {"Time (s)", "Diameter(m)"}, PlotRange → {{0, 0.0265}, {0, 4.0 * 10-6}},
  Frame → {True, True, True, True}, FrameLabel → {"Time (s)", "Diameter(m)"},
  FrameTicks → Automatic, BaseStyle → {FontSize → 12}]

```

InterpolatingFunction[  Domain: {{0., 0.0276}}
Output: scalar]



According to this analysis, the droplet will have completely evaporated 0.0265 s after passing screen position 1, which is 13.25 in past screen position 1 and 35.25 in from the nozzle release point.

In summary, according to this analysis the 0:1 EtOH:H₂O droplet has an initial diameter of 4.0 μm, 3.72 μm after passing screen position 1 while exposed to 100% RH (0.044s of travel time), and will reach complete evaporation ~5 inches short of screen position 3 while exposed to 85% RH. This analysis shows that the 0:1 droplet will be evaporated 0.0705 s after leaving the nozzle release point.

-----*****-----

EVAPORATION OF 1:3 ETHANOL:WATER DROPLET [@77F=25C=298.15K, & 100% RH] ;
 (used Rault's Law of mixtures to determine the vapor pressure of the ethanol/water solution);

```

ClearAll[Local]
M = .0206357;
Dv = 22.79 * 10-6;
Δp = 3556.099 - 3132.41;
d0 = 4 * 10-6;
ρ = 965.65;
R = 8.3144;
Tf = 298.15;
a = - (4 M * Dv) * Δp;
b = ρ * R * Tf;

diam = NDSolve[{d'[t] == a/b, d[0] == 4 * 10-6}, d, {t, 0.0, 2}, MaxSteps -> 2 000 000];

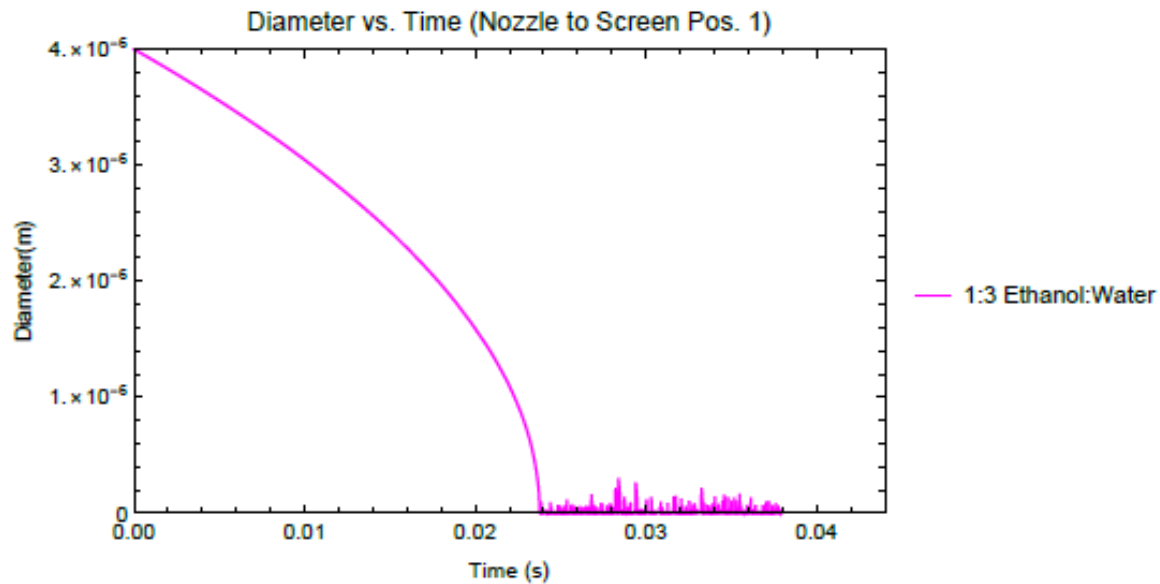
```

NDSolve: At t == 0.03793361363869671, step size is effectively zero; singularity or stiff system suspected.

```

solution = diam[[1, 1, 2]];
plot2a = Plot[solution[t], {t, 0., 0.044},
  PlotLegends -> LineLegend[{Magenta}, {"1:3 Ethanol:Water"}],
  PlotStyle -> {Magenta}, PlotLabel -> "Diameter vs. Time (Nozzle to Screen Pos. 1)",
  PlotRange -> {{0, 0.044}, {0, 4.0 * 10-6}}, Frame -> {True, True, True, True},
  FrameLabel -> {"Time (s)", "Diameter(m)"},
  FrameTicks -> Automatic, BaseStyle -> {FontSize -> 12}]

```



This plot shows us that 1:3 Ethanol:Water droplets should have fully evaporated before reaching screen position 1, while only being exposed to 100% RH.

```

ClearAll[Local]
M = .0206357;
Dv = 22.79 * 10-6;
Δp = 3556.099 - 3132.41;
d0 = 4 * 10-6;
ρ = 965.65;
R = 8.3144;
Tf = 298.15;
a = - (4 M * Dv) * Δp;
b = ρ * R * Tf;

diam = NDSolve[{d'[t] == a/b, d[0] == 4 * 10-6}, d, {t, 0.0, 2}, MaxSteps -> 2000000];

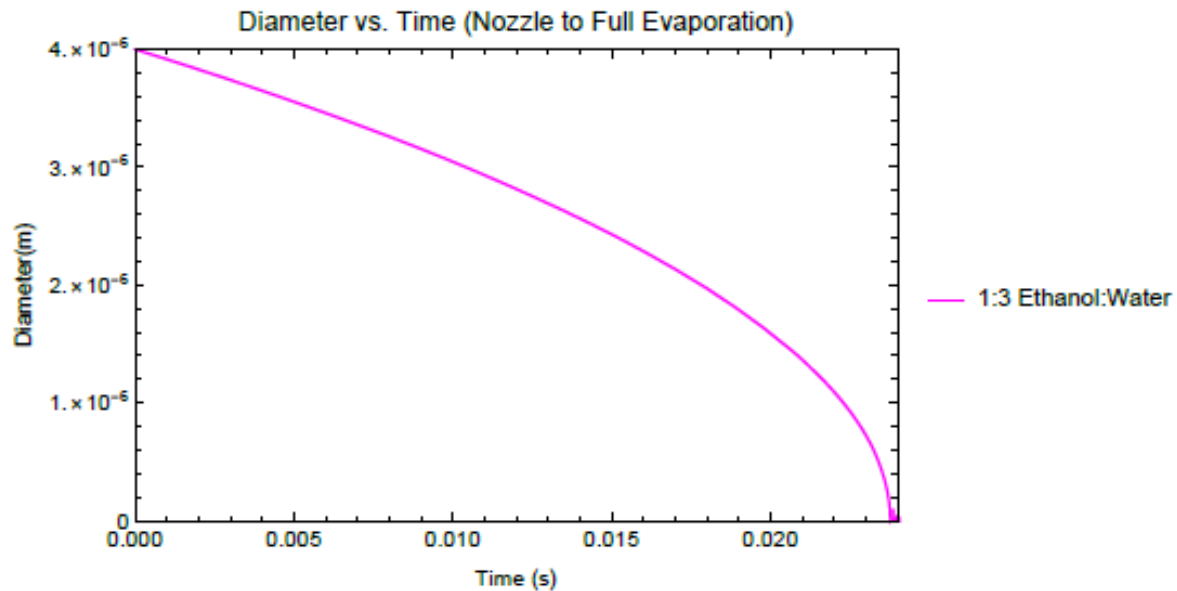
```

⋮ NDSolve: At t == 0.03793381363869671, step size is effectively zero; singularity or stiff system suspected.

```

solution = diam[[1, 1, 2]];
plot2b = Plot[solution[t], {t, 0., 0.044},
  PlotLegends -> LineLegend[{Magenta}, {"1:3 Ethanol:Water"}], PlotStyle -> {Magenta},
  PlotLabel -> "Diameter vs. Time (Nozzle to Full Evaporation)",
  PlotRange -> {{0, 0.024}, {0, 4.0 * 10-6}}, Frame -> {True, True, True, True},
  FrameLabel -> {"Time (s)", "Diameter(m)"},
  FrameTicks -> Automatic, BaseStyle -> {FontSize -> 12}]

```



According to this analysis, the 1:3 Ethanol:Water droplet will have completely evaporated 0.0238 s after being released, which corresponds to ~12 inches, or about halfway to screen position 1 while only being exposed to 100% RH.



EVAPORATION OF 1:1 ETHANOL:WATER DROPLET [077F=25C=298.15K, & 100% RH];;
 (used Raoult's Law of mixtures to determine the vapor pressure of the ethanol/water
 solution);
 (used "Molar Average Diffusivity")

```
ClearAll[Local]
```

```
M = .0246;
```

```
Dv = 20.9 * 10-6;
```

```
Δp = 4277.17 - 3132.41;
```

```
d0 = 4 * 10-6;
```

```
ρ = 926.5;
```


```
R = 8.3144;
```

```
Tf = 298.15;
```

```
a = - (4 M * Dv) * Δp;
```

```
b = ρ * R * Tf;
```

```
diam = NDSolve[{d'[t] ==  $\frac{a}{d[t]}$ , d[0] == 4 * 10-6}, d, {t, 0.0, 2}, MaxSteps -> 2 000 000]
```

 **NDSolve:** Maximum number of 2000000 steps reached at the point t == 0.023643588188058055.

```
{ {d -> InterpolatingFunction[ Domain: {{0., 0.0236}}  
Output: scalar ] } }
```

EVAPORATION OF 1:0 ETHANOL:WATER DROPLET [077F=25C=298.15K, & 80% RH]::

```
ClearAll[Local]
```

```
M = .04606844 ;
```

```
Dv = 11 * 10-6 ;
```

```
Δp = 133.322368 * 59.2 ;
```

```
d0 = 4 * 10-6 ;
```

```
ρ = 789 ;
```

```
R = 8.3144 ;
```

```
Tf = 298.15 ;
```

```
a = - (4 M * Dv) * Δp ;
```

```
b = ρ * R * Tf ;
```

```
diam = NDSolve[{{d'[t] ==  $\frac{a/b}{d[t]}$ , d[0] == 4 * 10-6}, d, {t, 0.0, 2}, MaxSteps -> 2 000 000]
```

NDSolve: At t == 0.0017198700572298156, step size is effectively zero; singularity or stiff system suspected.

```
{{d -> InterpolatingFunction[  Domain: {{0., 0.00172}} Output: scalar ]}}
```

```
solution = diam[[1, 1, 2]] ;
```

```
plot5a = Plot[solution[t], {t, 0., 0.044},
```

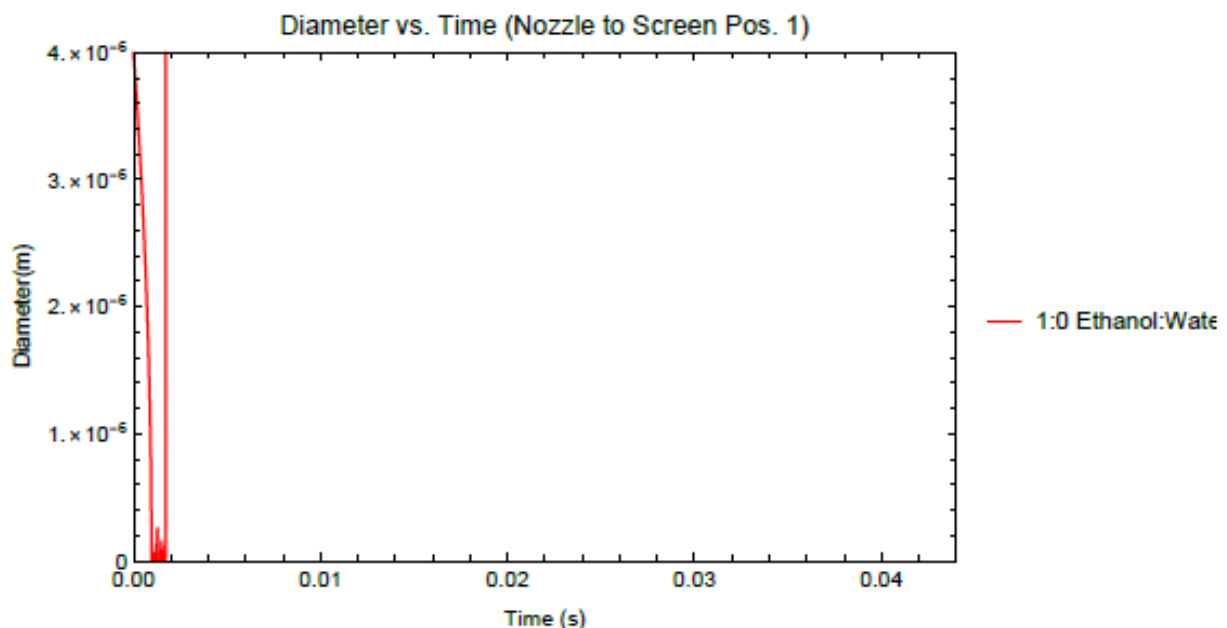
```
PlotLegends -> LineLegend[{Red}, {"1:0 Ethanol:Water"}], PlotStyle -> {Red},
```

```
PlotLabel -> "Diameter vs. Time (Nozzle to Screen Pos. 1)",
```

```
PlotRange -> {{0, 0.044}, {0, 4.0 * 10-6}}, Frame -> {True, True, True, True},
```

```
FrameLabel -> {"Time (s)", "Diameter(m)"},
```

```
FrameTicks -> Automatic, BaseStyle -> {FontSize -> 12}]
```



This plot shows us that 1:0 Ethanol:Water droplets should have fully evaporated before reaching screen position 1 while exposed to 100% RH.

```

ClearAll[Local]
M = .04606844;
Dv = 11 * 10-6;
Δp = 133.322368 * 59.2;
d0 = 4 * 10-6;
ρ = 789;
R = 8.3144;
Tf = 298.15; a = - (4 M * Dv) * Δp;
b = ρ * R * Tf;
diam = NDSolve[{d'[t] == a/b, d[0] == 4 * 10-6}, d, {t, 0., 2}, MaxSteps → 2 000 000]

```

ⓘ NDSolve: At t == 0.0017198700572298156, step size is effectively zero; singularity or stiff system suspected.

```

{{d → InterpolatingFunction[

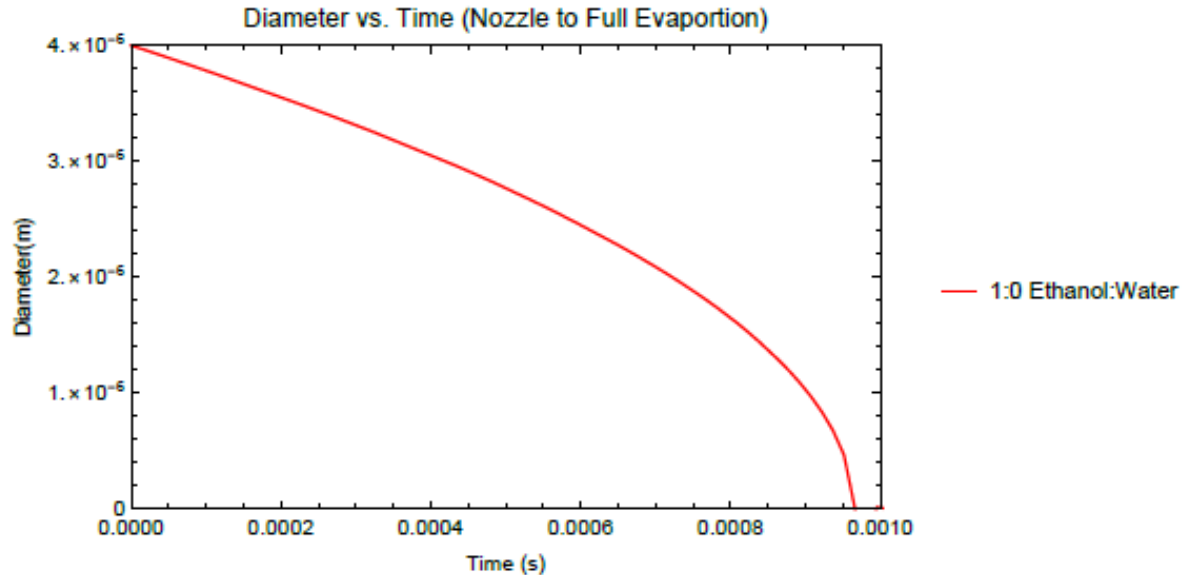
```



```

solution = diam[[1, 1, 2]];
plot5b = Plot[solution[t], {t, 0., 0.0044},
  PlotLegends → LineLegend[{Red}, {"1:0 Ethanol:Water"}], PlotStyle → {Red},
  PlotLabel → "Diameter vs. Time (Nozzle to Full Evaporation)",
  PlotRange → {{0, 0.001}, {0, 4.0 * 10-6}}, Frame → {True, True, True, True},
  FrameLabel → {"Time (s)", "Diameter(m)"},
  FrameTicks → Automatic, BaseStyle → {FontSize → 12}]

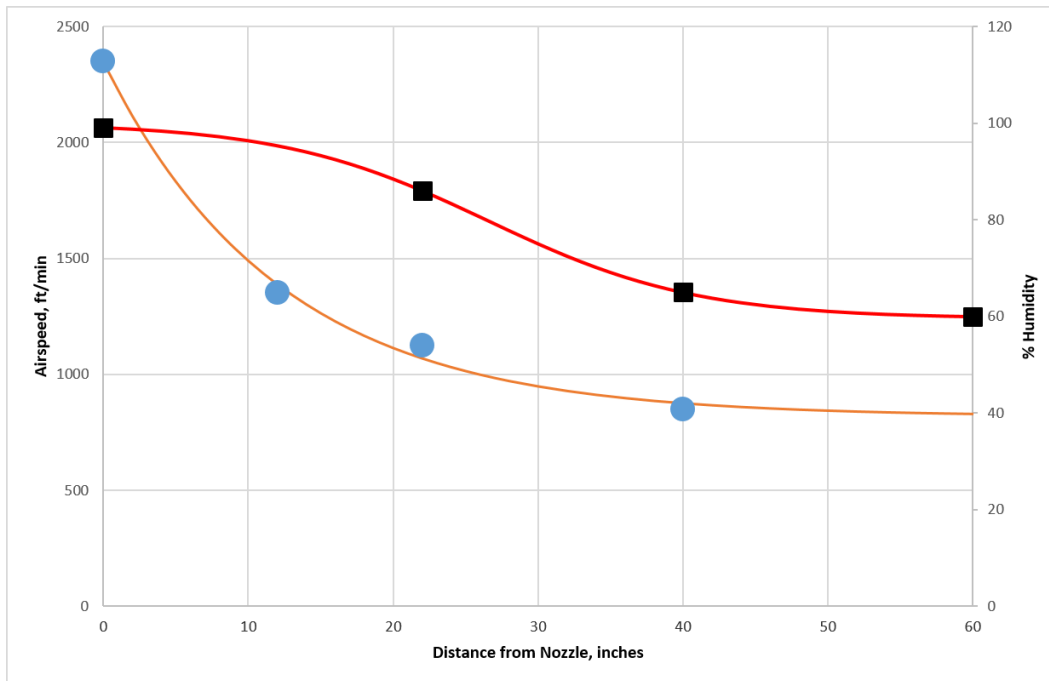
```



According to this analysis, the 1:0 Ethanol:Water droplet will have completely evaporated 0.001 s after being released, which corresponds to 0.5 inches past the nozzle release point and 100% RH.

Appendix D: Measured Airspeed and Relative Humidity Values in the Contamination Rig

Airspeed and humidity were collected in the contamination rig using a standard temperature/humidity sensor and a hand-held anemometer.



REPORT DOCUMENTATION PAGE

Form Approved
OMB No. 0704-0188

The public reporting burden for this collection of information is estimated to average 1 hour per response, including the time for reviewing instructions, searching existing data sources, gathering and maintaining the data needed, and completing and reviewing the collection of information. Send comments regarding this burden estimate or any other aspect of this collection of information, including suggestions for reducing the burden, to Department of Defense, Washington Headquarters Services, Directorate for Information Operations and Reports (0704-0188), 1215 Jefferson Davis Highway, Suite 1204, Arlington, VA 22202-4302. Respondents should be aware that notwithstanding any other provision of law, no person shall be subject to any penalty for failing to comply with a collection of information if it does not display a currently valid OMB control number.
PLEASE DO NOT RETURN YOUR FORM TO THE ABOVE ADDRESS.

1. REPORT DATE (DD-MM-YYYY) 1-06-2018		2. REPORT TYPE Technical Memorandum		3. DATES COVERED (From - To)	
4. TITLE AND SUBTITLE Mitigation of Polystyrene Microsphere Surface Contamination for Wind Tunnel Applications				5a. CONTRACT NUMBER	
				5b. GRANT NUMBER	
				5c. PROGRAM ELEMENT NUMBER	
6. AUTHOR(S) Wohl, Christopher, J.; Tiemsin, Pacita I.; Robbins, Samuel J.; Page, Ashle				5d. PROJECT NUMBER	
				5e. TASK NUMBER	
				5f. WORK UNIT NUMBER 147016.03.07.01.11.02	
7. PERFORMING ORGANIZATION NAME(S) AND ADDRESS(ES) NASA Langley Research Center Hampton, VA 23681-2199				8. PERFORMING ORGANIZATION REPORT NUMBER L-20930	
9. SPONSORING/MONITORING AGENCY NAME(S) AND ADDRESS(ES) National Aeronautics and Space Administration Washington, DC 20546-0001				10. SPONSOR/MONITOR'S ACRONYM(S) NASA	
				11. SPONSOR/MONITOR'S REPORT NUMBER(S) NASA-TM-2018-219835	
12. DISTRIBUTION/AVAILABILITY STATEMENT Unclassified Subject Category 23 Availability: NASA STI Program (757) 864-9658					
13. SUPPLEMENTARY NOTES					
14. ABSTRACT Polystyrene latex (PSL) microspheres have been utilized as seed material for flow visualization in wind tunnels. PSL microspheres, however, have been observed to strongly adhere to wind tunnel and model surfaces. Surface contamination of the cleaning screens, utilized to remove vorticity and provide laminar flow in the test section, is particularly problematic. Agglomeration of particles on these screens may cause constriction of the airflow through the screen resulting in inconsistent airflow properties in the test section. The adhesion mechanism of PSL microspheres to wind tunnel screens and flat plates, stainless steel 316, was evaluated in a contamination apparatus where small sections of screen material were exposed to PSL-seeded airflow. Airflow seeding parameters were changed using a design of experiments (DOE) methodology to evaluate how these changes affected the degree of surface contamination. The solution composition, comprised of ethanol and water, was determined to be the most significant factor in particle adhesion. Utilizing image analysis software, data were collected from the contaminated surfaces and were incorporated to generate predictive particle contamination models. A relationship was identified between the solvent evaporation rate and the morphology and magnitude of PSL contaminants on the test surfaces. This analysis can be extended to other solvent mixtures and may provide insight into simultaneously improving wind tunnel testing capabilities while diminishing facility contamination.					
15. SUBJECT TERMS Adhesion; Contamination; Particle image velocimetry; Seeded airflow					
16. SECURITY CLASSIFICATION OF:			17. LIMITATION OF ABSTRACT	18. NUMBER OF PAGES	19a. NAME OF RESPONSIBLE PERSON
a. REPORT	b. ABSTRACT	c. THIS PAGE			STI Help Desk (email: help@sti.nasa.gov)
U	U	U	UU	50	19b. TELEPHONE NUMBER (Include area code) (757) 864-9658